INFORMATION TO USERS

This manuscript has been reproduced from the microfilm master. UMI films the text directly from the original or copy submitted. Thus, some thesis and dissertation copies are in typewriter face, while others may be from any type of computer printer.

The quality of this reproduction is dependent upon the quality of the copy submitted. Broken or indistinct print, colored or poor quality illustrations and photographs, print bleedthrough, substandard margins, and improper alignment can adversely affect reproduction.

In the unlikely event that the author did not send UMI a complete manuscript and there are missing pages, these will be noted. Also, if unauthorized copyright material had to be removed, a note will indicate the deletion.

Oversize materials (e.g., maps, drawings, charts) are reproduced by sectioning the original, beginning at the upper left-hand corner and continuing from left to right in equal sections with small overlaps.

Photographs included in the original manuscript have been reproduced xerographically in this copy. Higher quality 6" x 9" black and white photographic prints are available for any photographs or illustrations appearing in this copy for an additional charge. Contact UMI directly to order.

UMI®

UNIVERSITY OF ALBERTA

Erbium/Ytterbium Co-doped Planar Waveguide Amplifiers: Modeling and Fabrication

BY

Ratnambikai Shankar ©

A thesis submitted to the Faculty of Graduate Studies and Research in partial fulfillment of the requirements for the degree of **Master of Science**.

DEPARTMENT OF ELECTRICAL AND COMPUTER ENGINEERING

EDMONTON, ALBERTA, CANADA
SPRING, 2001

Canada

UNIVERSITY OF ALBERTA

LIBRARY RELEASE FORM

NAME OF AUTHOR: **Ratnambikai Shankar**

TITLE OF THESIS: **Erbium/Ytterbium Co-doped Planar Waveguide Amplifiers: Modeling and Fabrication**

DEGREE: **Master of Science**

YEAR THIS DEGREE GRANTED: 2001

T. Rat____
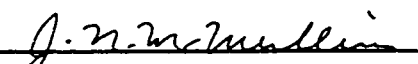
1112, 1339 Meadowlands Dr East

Nepean, Ontario, Canada

K2E 7B4

DATE: _January 30, 2001_

UNIVERSITY OF ALBERTA

FACULTY OF GRADUATE STUDIES AND RESEARCH

The undersigned certify that they have read, and recommend to the Faculty of Graduate Studies and Research for acceptance, a thesis entitled **Erbium/Ytterbium Co-doped Planar Waveguide Amplifiers: Modeling and Fabrication** submitted by **Ratnambikai Shankar** in partial fulfillment of the requirements for the degree of **Master of Science.**

J. N. McMullin, Supervisor

R. DeCorby, Co-Supervisor

S. Robinson

R. Marchand

DATE: Jan. 29, 2001.

Acknowledgments

First, I would like to express my deepest gratitude to my supervisors, Dr. James N. McMullin and Dr. Ray DeCorby, who have given me an opportunity to pursue my graduate studies in the area of photonics under their supervision at the University of Alberta. I thank them for their guidance, advice, and support in every aspect.

Additionally I thank Dr. Chris Haugen who shared his knowledge through technical discussions, encouraged and supported me throughout this work.

To the staff at Micro Fabrication Facilities, Dr. Ken Westra, Nicole Morin, and Keith Franklin, the training they have provided me in developing the devices is greatly appreciated. I also thank Dr. James Broughton at Micralyne for his technical support.

There are many individuals who helped me in innumerable ways in fabricating the devices and setting up the instruments for the measurements. They include David Clegg, Craig Unick, Kevin Partridge, Scott Kennedy, Travis Robinson and Hue Nguyen.

My special thanks are to George Braybrook, who helped in imaging the waveguides and Lang Shi, who helped in analyzing the glass samples.

I am thankful to the Telecommunication Research Laboratories (TRLabs) for the financial support and the laboratory facilities in carrying out my work. As well, my thanks go to the wonderful staff and to my colleagues at TRLabs for providing a pleasant environment for my studies.

I am very grateful to my parents, brother, and sisters for their love and support over the years.

Finally, I thank my loving husband, Kana Shankar, for his patience, encouragement, and support throughout this work.

For my family and my husband

Abstract

In recent years, Erbium (Er)-doped waveguide amplifiers have attracted increasing attention since they can be used to compensate the losses of other functional passive devices, such as splitters, combiners, filters, and multiplexers, in realizing high-density optical integrated circuits operating at a wavelength of 1.55 μm. Such circuits have potential applications in the areas of optical telecommunication and signal processing. This work describes the operation, modeling, and fabrication of Er-doped waveguide amplifiers.

A numerical model to predict the gain characteristics of a heavily doped waveguide amplifier is described. Amplifier noise and all possible gain-limiting mechanisms such as ion-ion interactions are included in the model. Simulation results show that co-doping with Ytterbium (Yb) overcomes the undesirable effects to some extent. Er/Yb co-doped waveguide amplifiers were fabricated using a commercially available laser glass by an electric-field-assisted ion-exchange technique. A gain of 1.4 dB over 0.5 cm waveguide is demonstrated.

Table of Contents

List of Tables

List of Figures

1. Introduction

1.1 Optical communication

In the telecommunication industry, information transfer by means of light waves started back in the 1980's following the invention of low-loss glass fibers. Since then, through several generations of development, the transmission rates have increased dramatically so that now more than 10^{12} bits per second (Terabits, Tb/s) can be transmitted over a single optical fiber at carrier wavelengths near 1.55 µm. Two major technical advances have contributed to this achievement. The first one is the introduction of Wavelength Division Multiplexing (WDM), which allows several independent information channels, each at slightly different wavelengths, to be transmitted simultaneously over a single fiber. Thus, in each single installed fiber, the traffic previously carried was then multiplied by the number of channels accommodated in the WDM scheme. The second advance was the successful development of Erbium (Er) Doped Fiber Amplifiers (EDFAs) which replaced the conventional electronic-based regenerator systems. The use of EDFAs not only helps to overcome the bandwidth (or bit rate) restrictions imposed by the electronic systems in the regenerators but also provides in-line optical amplification to all wavelength channels in the WDM scheme by a single EDFA.

EDFAs are widely used in long-haul fiber optic networks where the fiber loss, ~ 0.2 dB/km, is compensated periodically by placing EDFAs in the transmission link with spacings of up to 100 km. EDFAs make use of Er ions to provide the optical amplification at wavelengths near 1.55 µm, the long wavelength window dominantly used in fiber optic networks since the fiber loss is found minimum around this wavelength. Light from an external energy source at a wavelength of 980 nm or 1480 nm, coupled along with the information signal, is passed through the EDFA to excite the Er ions in order to produce the optical amplification through stimulated emission of photons at the signal wavelength.

Parallel to this development of EDFAs, much attention has also been focused on developing a smaller version of optical amplifiers, planar waveguide amplifiers, by several research groups [1]-[24]. While EDFAs have lengths of 30 m to 50 m, the planar

waveguide amplifiers should have dimensions on the order of few centimeters to be compatible with optical integrated circuits.

1.2 Integrated optics

An optical integrated circuit is generally designed to perform certain functions by integrating several optical devices, such as splitters, (de)multiplexers, combiners, modulators, and filters, together on one common planar substrate. The routing among the devices is often realized with planar optical waveguides. Although most of these functional devices are well developed as fiber-based devices, the benefits from high-density integrated circuitry appear to be more promising compared to circuits made of fiber components in meeting present and future technological demands. Some benefits are: reduced size and weight; flexibility in the design and fabrication of the devices; and compatibility with transceivers and electronic control circuitry [25],[26].

Optical integrated circuits can be categorized into two main groups, monolithic and hybrid. In the monolithic approach, a single substrate material is used to form all optical devices. In the hybrid approach, on the other hand, two or more substrate materials that are used for different devices are bonded together to combine all devices as a single unit. These two different techniques have their own merits and demerits.

The major advantage in hybrid integration is that it has the flexibility in piecing devices that have been substantially optimized for a given material and processing techniques. Also, it allows combining active devices such as lasers and detectors, which are mainly formed on semiconductor materials with other passive devices such as splitters and filters, which are mostly formed on dielectric materials. But a major drawback in this approach is that the bonds holding various elements are subject to misalignment because of vibration and thermal expansion. Monolithic optical integrated circuits are ideal; these are more stable and ultimately less expensive since mass production of circuits is possible by automated processing.

In optical integrated circuits, the light is manipulated locally as it passes through various functional devices and eventually the intensity of the light is reduced considerably. The accumulation of the insertion losses introduced by each device and in

2

cases where optical splitting is performed could bring the signal intensity down to a level where no further processing or distribution of the signal is possible. This effect calls for an active optical amplifying planar device to be inserted to the circuitry to boost the signal to a desired level.

1.3 Er-doped Planar waveguide amplifiers

Er-doped planar waveguide amplifiers have been demonstrated over the past few years and their amplifying characteristics are improving [2],[11],[12]. There have been reports demonstrating the successful integration of Er-doped waveguide amplifiers with other functional devices, such as a splitter [1] and a combiner [2].

The basic principles that govern optical amplification in Er-doped amplifiers, either in the form of fiber or waveguide, are the same. Nevertheless, the pump and signal interaction path (active length) is shorter in waveguide amplifiers due to its compact size. Thus, much higher doping levels are needed in waveguide amplifiers compared to that of fiber amplifiers in order to realize a reasonable amount of gain.

Silica has been the main raw material in fiber production. The solubility of Er ions in silica is limited to about 10^{24} ions/m^3 and above this limit clustering of ions appears and results in serious reduction in the amplifier efficiency [27]. Many different materials have been explored over the years in overcoming the solubility limitations in realizing high gain short waveguide amplifiers.

Like other integrated optical devices, waveguide amplifiers are fabricated using various thin-film processing techniques. The choices on fabrication techniques using various materials give rise to realizing different waveguide structures. This flexibility in the waveguide design is taken as an advantage in optimizing the amplifier gain in terms of waveguide structures and dimensions.

1.4 Outline of this work

This work can be divided into two main parts. One is the theoretical study related to waveguide amplifiers, given in Chapter 2, and the other is the experimental work done on developing Er-doped planar waveguide amplifiers, given in Chapters 3, 4 and 5.

Chapter 2 starts providing a theoretical background on light propagation on planar structures. An inside view of the optical amplification mechanism is given and the efficiency of the amplification process is discussed in detail. A numerical model for the Er-doped waveguide amplifier is then developed and verified against some experimental results. The amplifier characteristics are studied with the developed model in terms of various amplifier parameters.

In Chapter 3, the materials that have been used in realizing waveguide materials are reviewed. The bulk material characterization performed on two different glasses, referred to as stock and custom glass, both used in the fabrication of waveguide amplifiers, is given and the results obtained are presented and discussed.

In Chapter 4, various fabrication techniques for realizing waveguide amplifiers are reviewed. In particular, the ion-exchange technique that was used for device fabrication in this work is discussed in detail. The process steps carried out in fabricating Silver-Sodium (Ag^{+}-Na^{+}) ion-exchanged waveguides on the bulk glasses are given.

The optical characterization on the ion-exchanged waveguides formed on both glass samples is described in Chapter 5. The amplification characteristics of these waveguides are shown and discussed.

Finally, a conclusion on this overall work is given in Chapter 6.

2. Numerical modeling of planar waveguide amplifiers

A numerical model for predicting the characteristics of Er/Yb co-doped waveguide amplifier, operating in the 1550 nm wavelength region, is developed and validated by comparing the numerical results generated with the model and the experimental data reported in the literature. The model developed is then used for the detailed analysis of an Er/Yb co-doped waveguide amplifier in terms of various device parameters. The chapter starts by providing a general view and the necessary physical arguments related to light propagation in planar devices and the optical amplification mechanism before stepping into the model formulation, simulations, and discussion.

2.1 Light propagation in planar waveguide structures: theoretical background

The fundamental element in optical integrated circuits is an optical waveguide, a structure that is used to confine and guide light in optical devices. A very familiar waveguide in optical communication is the optical fiber, which has a circular cross-section. However, the structures that are of interest in integrated optics are planar waveguides. Generally, these planar waveguides are formed on a common substrate that functions as a platform for the integration of several devices. The simplest planar structure is a slab waveguide as shown Figure 2.1. It is characterized by three parallel layers infinite in extent with respect to one direction (x), where a core layer (refractive index n_2) is sandwiched between an upper cladding layer (refractive index n_1) and a lower cladding layer (refractive index n_3). Obviously, this slab waveguide can not be a practical waveguide due to its infinite dimensions. However, it can form the basis for understanding and analyzing the waveguiding properties of complicated three-dimensional practical waveguides.

In order to achieve light guidance in an optical waveguide it is necessary to have the relationship among the refractive indices as

$$n_2 > n_3, n_1. \tag{2.1}$$

When $n_3 = n_1$ the structure is called a symmetrical slab waveguide and if $n_3 \neq n_1$ we call it as an asymmetrical slab waveguide. Here, we analyze an asymmetrical slab waveguide

(i.e. $n_3 > n_1$) and the study of a symmetrical slab waveguide is then straightforward with the assumption of $n_3 = n_1$.
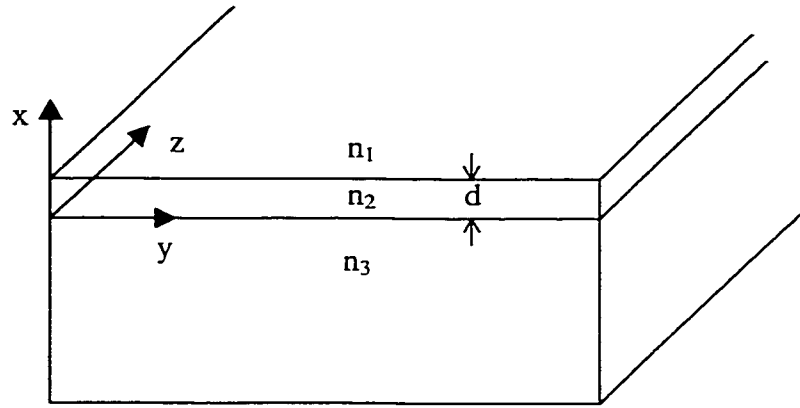
Figure 2.1 Schematic of a planar slab waveguide.

Optical waves are an electromagnetic phenomenon and they travel in any waveguiding media in distinct optical modes. A mode can be described as a spatial distribution of optical energy in one or more dimensions. An equivalent mathematical definition of a mode refers to a specific solution of Maxwell's equations that satisfies the appropriate boundary conditions of the given waveguide structure. For a linear, isotropic, nonconducting, and homogeneous medium with no free electric charges, the wave equation can be derived from Maxwell's Equations as

$$\nabla^2 E\ (r,t) = (n^2/c^2\ )\partial^2 E\ (r,t)/\partial t^2 \tag{2.2}$$

where E is the electric field vector, r is the radius vector, n is the index of refraction of the medium, c is the speed of light in a vacuum, and t is the time-dependent variable. For monochromatic waves, the solution to the Equation 2.2, can be given as

$$E\ (r)e^{j\omega t} \tag{2.3}$$

where ω is the sinusoidal frequency in radians and $j = \sqrt{-1}$. If we consider a sinusoidally-varying field propagating in the z direction, in Cartesian co-ordinates (x, y, z), then the electric field has the form

$$E\ (r) = E\ (x,y)e^{(-j\beta z)} \tag{2.4}$$

where β represents the propagation constant. Substituting Equations 2.3 and 2.4 in 2.1, the wave equation can be simplified to

$$\partial^2 E\ (x,y)/\partial x^2 + \partial^2 E\ (x,y)/\partial y^2 + (k^2 n^2 - \beta^2)\ E\ (x,y) = 0 \qquad (2.5)$$

where k, ($k = \omega/c$) is the wave number in free space. For two-dimensional slab waveguides, we assumed there is no variation in the y direction, which can be symbolically expressed as

$$\partial/\partial y = 0 \qquad (2.6)$$

Hence, by using Equation 2.6 the wave equation reduces to

$$\partial^2 E\ (x)/\partial x^2 + (k^2 n_i^{\ 2} - \beta^2)\ E\ (x) = 0 \qquad (2.7)$$

where n_i represents the refractive index of the ith region ($i=1,2,3$). A similar expression can also be derived from Maxwell's equation for the magnetic field $H\ (x)$ in the waveguide.

The solutions to Equation 2.7 are the distinct orthogonal modes [28] that propagate in the slab waveguide. These modes can be classified as Transverse Electric (TM) and Transverse Magnetic (TM) modes. TE modes do not have a component of the electric field in the direction of propagation, while TM modes do not have a magnetic component along the direction of propagation.

In this thesis we assume the incident light is a linearly polarized TE wave, i.e. $E_z=0$ (the subscript z denotes the direction of the field). For the slab waveguide the orthogonal set of coupled fields for the TE wave is $\{E_y,\ H_z,\ H_x\}$. If we can determine one of these fields, the other two can be obtained through the relationship found in Maxwell's equations. From Equation 2.7, we see the solutions for the electric field are either sinusoidal or exponential functions of x in all three regions, depending on whether the term $(k^2 n_i^{\ 2} - \beta^2)$, $i=1,2,3$, is greater than or less than zero. Also, any valid solution must satisfy the boundary condition at the two interfaces at x=0 and x=d. Hence, the tangential components, E_y and H_z ($H_z \propto \partial E_y/\partial x$), should be continuos at x=0 and x=d. Therefore, the possible modes are limited to those as shown in Figure 2.2. Let us analyze the solutions one by one as β takes values in the range from zero up to a value greater than kn_2 ($kn_2 > kn_3 > kn_1$, since $n_2 > n_3 > n_1$).

7
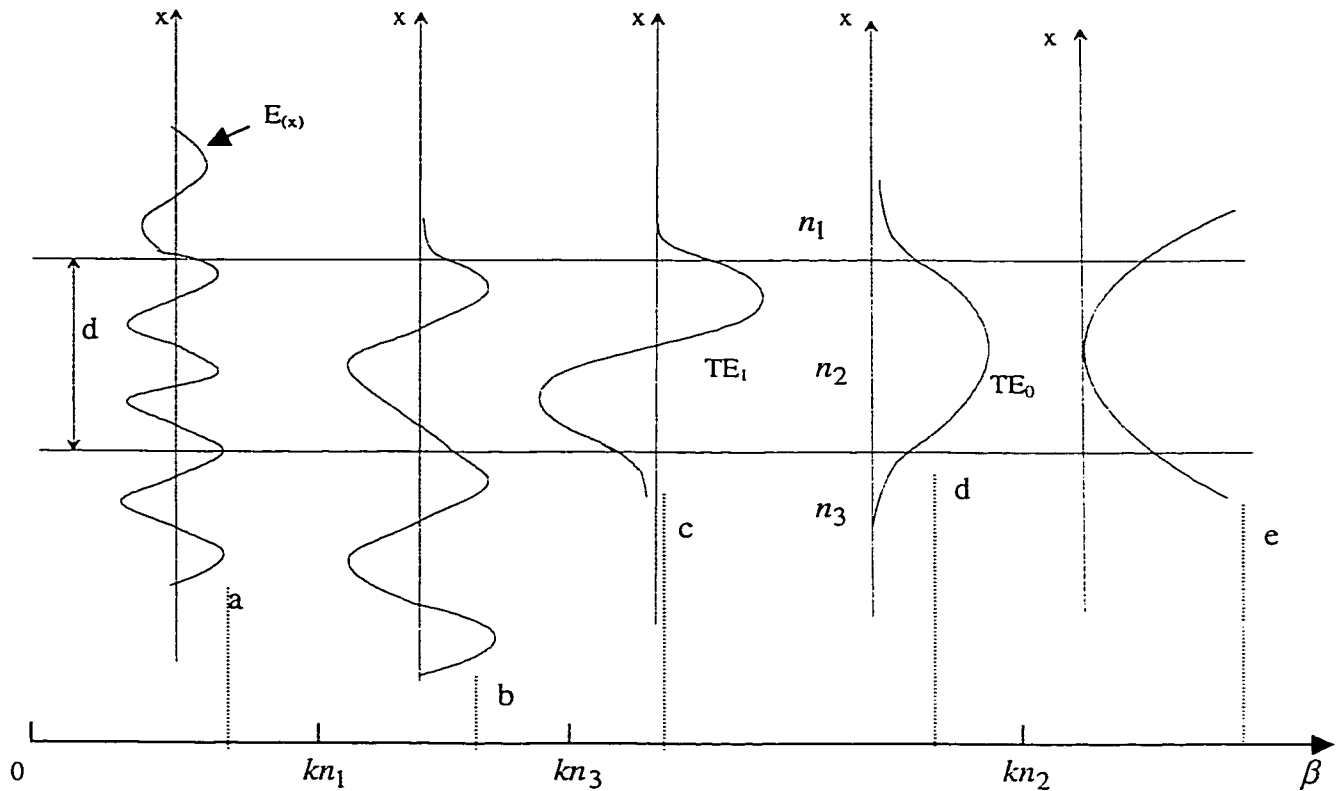
Figure 2.2 Illustration of possible modes in a slab waveguide.

- When $\beta < kn_1$, the solution for $E_{(x)}$ is oscillatory in all three regions in the waveguide and the mode shape, shown as (a) in Figure 2.2, will result. Since these modes are not guided and the energy is free to spread out to the cladding layers, these are referred to as radiation modes.

- If β lies between kn_1 and kn_3 ($kn_1 < \beta < kn_3$) then the modes (shown as (b)) are confined by the upper core-cladding interface, where the electric field exponentially decays to zero but they are sinusoidally varying in the lower cladding region. These modes loose energy from the waveguide to the lower cladding as they propagate and they tend to be damped out over a short distance. These modes are often called substrate radiation modes as in many cases the substrate functions as the lower cladding.

8

- When β falls between kn_3 and kn_2 ($kn_3 < \beta < kn_2$) mode shapes such as (c) and (d) will result, where the modes are well confined at both interfaces. These are the useful modes that can be guided and propagated through the waveguide structure. These guided modes are generally numbered according to how many field zeros occur in the core region. Hence, the mode shape (c) is referred as the zero order mode or the fundamental mode (TE$_0$) and the mode shape (d) is referred as the first order mode (TE$_1$).

- When $\beta > kn_2$, the solutions are exponential in all three regions and a mode shape (e) will result. This mode is not realizable in nature because the fields are increasing exponentially in the cladding layers implying infinite energy.

Basically, the theory and the underlying mode structures that we have seen for the slab waveguide are similar to any type of waveguide structures. In most practical applications, the waveguides used for integrated optics are channel waveguides where the light is confined in two transverse directions, x and y, while the light is guided along the z direction. Consequently, the field vectors are now functions of x and y (e.g. E (x, y), H (x, y)) and the mathematical treatment becomes complicated and lengthier. There are various analytical approaches that have been developed to solve the field solutions in complicated channel waveguide structures. These include Effective Index Method [29], Marcatilli [30], Multi-Grid Finite Difference [31] and Film Mode Matching [32]. In this thesis, commercially available numerical modeling software, BBV Selene [33] was used to generate the field profiles in structures that are of interest for the modeling of waveguide amplifiers. Among the various numerical methods which are available in this software, the Multi-Grid Finite Difference method was chosen for calculation of field profiles presented in this thesis. This method is a full vectorial method and it supports adaptive grid spacing with grid points occurring at the core-cladding boundary. The generated field profiles (amplitude of the electric field in each grid point across the waveguide structure) were exported as text files and then used for the calculation of intensity profiles and running simulations of waveguide amplifiers, as will be described in Section 2.5.

9

2.2 Optical amplification

Optical amplifiers make use of rare-earth elements, such as Er, Yb, Ho, Nd, and Pr, as a gain medium by doping the base material with these elements. In most of the materials, rare-earth (RE) ions assume the trivalent charge state (RE^{3+}) of [Xe] $4f^{N-1}5s^2\ 5p^6 6s^0$, where [Xe] represents the closed shell configuration of Xe [34]. In this ion configuration one electron from the 4f shell and two electrons from the 6s shell are removed and the inner electrons of the 4f shell are shielded by the outermost shells 5s, and 5p. Spin-spin and spin-orbit coupling of electrons in the 4f shell give rise to a number of energy levels useful for laser transitions in the medium. Different rare-earth ions can be used to realize optical amplification at different wavelengths covering a wide range from 0.5 to 3.5 µm [35]. Er-doped optical amplifiers are the most attractive in telecommunication applications because its emission wavelength is around 1550nm, a wavelength, mainly used for fiber optic communication.

A simple illustration of the amplification process in an Er^{3+} doped system is shown in Figure 2.3. For easy reference, the energy levels of the Er^{3+} ions are named as E_1 (ground state or zero energy state), E_2 (intermediate state), and E_3 (high energy state). In the absence of any electromagnetic energy in the medium, the ions reside at zero energy level, shown as in Figure 2.3 (a). These ions can be excited and moved to the higher energy level, E_3, through the absorption of an incoming photon if the photon energy $h\upsilon$ (where h is a Planck's constant and υ is the frequency of incident light) is equal to the energy difference E_3-E_1, Figure 2.3 (b). These excited ions subsequently decay to a more stable energy level, referred as *metastable* state, E_2, via a non-radiative relaxation (by releasing some energy in the form of heat). The ions in this level then return to the ground state by releasing their energy in the form of new photons. This emission process may occur in two different ways, called spontaneous emission and stimulated emission. In the case of spontaneous emission (c), the emitted photons have random characteristics with no relationships among them. In the case of stimulated emission (d), the ions are triggered by an existing signal photon with energy equal to E_2-E_1. The photons emitted in this process are an exact replica of the triggering photon in frequency, phase, and polarization. These newly generated photons through the

stimulated emission process add more and more power to the initial trigging signal as it passes through and results in optical amplification. In contrast, the spontaneous or random emission results in noise in the amplifying device.
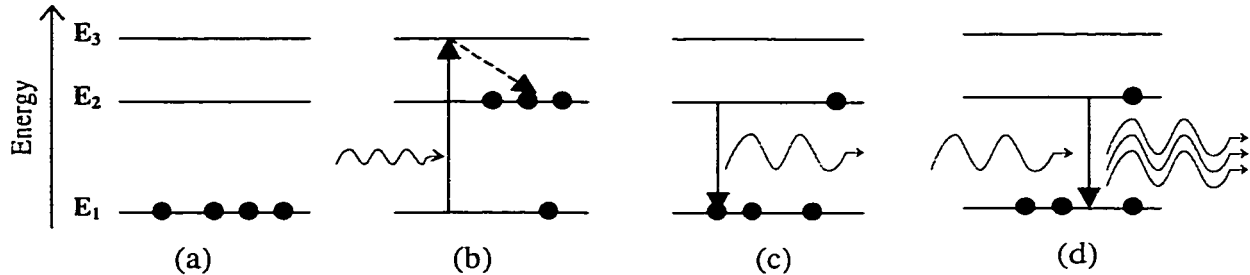
Figure 2.3 An illustration of the optical amplification process. (a) The ions are at zero energy state. (b) Excitation to higher energy level through the absorption of an incoming photon and subsequent relaxation to intermediate energy level. (c) Spontaneous emission. (d) Stimulated emission. The black dots indicate the state of the ion.

The necessary requirement for realizing optical amplification is to maintain a population inversion between the states that are relevant to the stimulated emission process, i.e., the number of ions in the E_2 energy state should be grater than the number of ions in the ground state. This can be achieved by supplying sufficient optical power at the appropriate wavelength using an external energy source, often referred to as the *pump*. Another critical factor for efficient optical amplification is how long the excited ions can stay in the metastable state until they get a chance to be triggered by a signal photon. This duration is referred as the *lifetime* and defined as the inverse of exponential decay rate at which the ion population decays from the metastable state to ground state by means of spontaneous transition or non-radiative transition. Depending on the host material, the lifetime for Er^{3+} ions can be as high as ~20 ms.
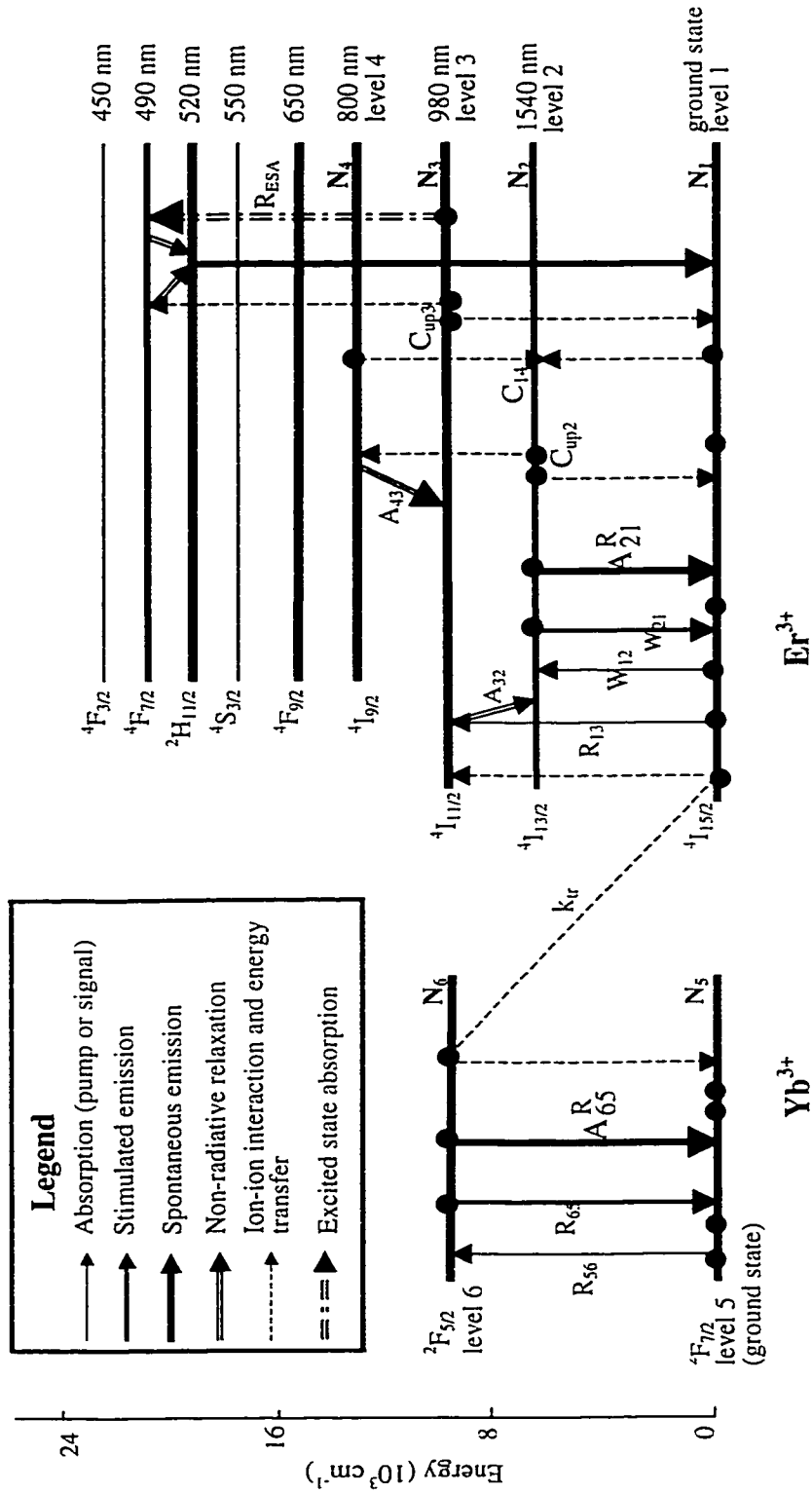
Figure 2.4 Energy level diagram for a Er/Yb co-doped laser host. The black dots indicate the state of the ions and arrowheads indicate the possible transitions in the system.

2.3 Amplifier efficiency

The overall performance of any optical amplifier is determined by several factors. These include doping level and solubility of the active ions in the waveguiding material, optical characteristics of the active ion such as the emission and absorption cross-sections at both pump and signal wavelengths and the lifetime of the metastable state, and pump and signal intensity distribution across the waveguiding region. In addition to all these, especially in heavily doped amplifiers where the inter-ionic distance is reduced significantly, the effect of ion-ion coupling between two neighboring ions has been shown to decrease the efficiency of the amplifier severely [3],[27].

2.3.1 Energy level diagram for an Er/Yb co-doped system

Figure 2.4 shows the energy diagram for an Er/Yb co-doped laser host indicating the levels up to 24×10^{3} cm^{-1}. The energy levels (or the manifold) are labeled with the Russell-Saunders notation and for each energy level the corresponding transition wavelength is also marked. The arrows indicate the possible transitions (nature of transition is shown in the legend) among energy levels. Each of these transitions and the relevant effects are described in subsequent sections. The parameters given to each transition are used to develop a numerical model, as will be described in Section 2.4. The appropriate pump wavelength region, common for both Er^{3+} and Yb^{3+} ions, is around 980 nm. The light emission for Er^{3+} ions at wavelength around 1550 nm occurs from the first excited energy state, $^{4}I_{13/2}$ (or the metastable state) to the ground state. As studied in Section 2.2, only the stimulated emission from the metastable state produces optical gain and the gain produced scales with the number of ions in the metastable state. Any other process that removes the ions from this state therefore decreases the efficient operation of the amplifier.

2.3.2 Co-operative upconversion

Co-operative upconversion is the most severe gain-limiting factor in heavily doped amplifiers (Er concentrations above 10^{25}-10^{26} ions/m^{3}). At high concentrations, the distance between Er^{3+} ions become small and two neighboring ions tend to cross-relax with each other. One such process is shown with a parameter C_{up2} (Figure 2.4), where

13

two ions in $^4I_{13/2}$ state interact, one transfers its energy to other, returning to the ground state and exciting the other ion to the higher energy state $^4I_{9/2}$. The ion moved to $^4I_{9/2}$ then relaxes non-radiatively to $^4I_{11/2}$ and the net result of the process is one excitation of Er^{3+} to the $^4I_{13/2}$ level is converted into heat. A similar process can also occur at the $^4I_{11/2}$ pump state (C_{up3}). In this process both of the excited ions that could relax to the $^4I_{13/2}$ state are lost. One falls to the ground state and the other moves up to $^4F_{7/2}$ state, followed by a rapid relaxation to $^2H_{11/2}$. From this state, the ion then decays straight to the ground state through the emission of photons at wavelengths around 520 nm (green light). Since co-operative upconversion requires two interacting ions in the excited states it is observable only when the pump power is high enough to maintain a high concentration of excited Er^{3+} ions.

The effect of this upconversion process not only depends on the exact Er concentration levels but also on the homogeneous distribution of the ions in the host material. A very efficient co-operative upconversion process can also occur when two ions form a cluster, resulting in almost immediate interaction of the ions once both of them are excited [4]. This is referred as the pair-induced upconversion. The inefficiency due to the clustering effect, however, can be overcome by choosing the appropriate host material where homogeneous distribution of ions could be achieved.

Another cross-relaxation mechanism that can be observed is shown by C_{14} and is just the opposite of co-operative upconversion. Here, one ion in the $^4I_{9/2}$ state cross-relaxes with an ion in the ground state and brings itself and the other to the $^4I_{13/2}$ state. Though the net result of this process is positive, due to the low population level found at $^4I_{9/2}$ state, the probability of occurrence of this process is minimal.

2.3.3 Excited State Absorption (ESA)

Excited Sate Absorption (ESA) is another gain-limiting factor [3],[5]. In ESA, pump absorption occurs not from the ground state of the Er^{3+} ions, but from an excited level whenever there is an appropriate energy gap available for the absorption of a pump photon. One such ESA, for the 980 nm pumping scheme, is shown in Figure 2.4 by R_{ESA}, where an excited Er^{3+} ion at $^4I_{11/2}$ state brings itself to a higher energy state, $^4F_{7/2}$, through the absorption of a pump photon. The ion moved to high-energy state subsequently relaxes to a lower level, $^2H_{11/2}$, and decays to the ground state through a green light emission around 520 nm. Unlike co-operative upconversion, since one ion is involved, ESA can occur only at high pump powers. The lifetime for the excited ions in the state where the ESA originates is also a factor that influences this effect. The effect of ESA results in non-linear pump absorption in the amplifying device and eventually limits the pump power conversion into useful signal amplification.

2.3.4 Amplified Spontaneous Emission (ASE)

The presence of spontaneous emission degrades the performance of the amplifier by adding unwanted power near the signal wavelength in the form of noise. Such spontaneously emitted photons subsequently get multiplied by the amplifier and travel along with the signal. The noise generated is hence referred as Amplified Spontaneous Emission (ASE). The ASE noise power generated travels in both directions of the waveguide due to its random nature of emission. Also, the ASE covers a broad spectral range. In the free ion the energy levels are sharp. But in solids, due to the Stark effect, each energy level splits into a manifold of energy sub-levels [34]. Therefore, the spontaneous emission of photons (for which no triggering signal is needed, Sec 2.2) naturally originates over a wavelength range, determined by the sub-level energy separation within each main level. The spreading of the ASE spectra often takes the shape of the emission cross-section spectra for Er^{3+} ions in the signal band as the amplified (noise) emission scales with the emission cross-section for Er^{3+} ions.

15

2.3.5 Ytterbium (Yb) sensitiza tion

As seen in previous sections, both upconversions and ESA significantly reduce the pumping efficiency for optimum signal amplification. One way to overcome this effect is to introduce another rare-earth, called a donor or sensitizer, which can effectively transfer its energy to Er^{3+} ions to improve the signal amplification. A well-known co-dopant for Er-doped amplifiers and lasers is Yb together with a pumping at 980 nm, the shared absorption wavelength by both ions [6]-[8],[34],[36]. Yb^{3+} ions in the ground state, $^2F_{7/2}$, absorb the pump photons and get excited to the $^2F_{5/2}$ energy state (Figure 2.4). The excited Yb^{3+} ion (sensitizer) then may transfer its energy to a nearby ground state Er^{3+} ion and excite the Er^{3+} indirectly to the $^4I_{11/2}$ pump state. A fast non-radiative decay of Er^{3+} ion from this pump level to the metastable state prevents any significant back-transfer of energy to a ground state Yb^{3+} ion. This cross-relaxation mechanism is shown with a parameter k_{tr}, where k_{tr} represents the forward energy transfer that results in populating the $^4I_{11/2}$ state of the Er^{3+} ions.
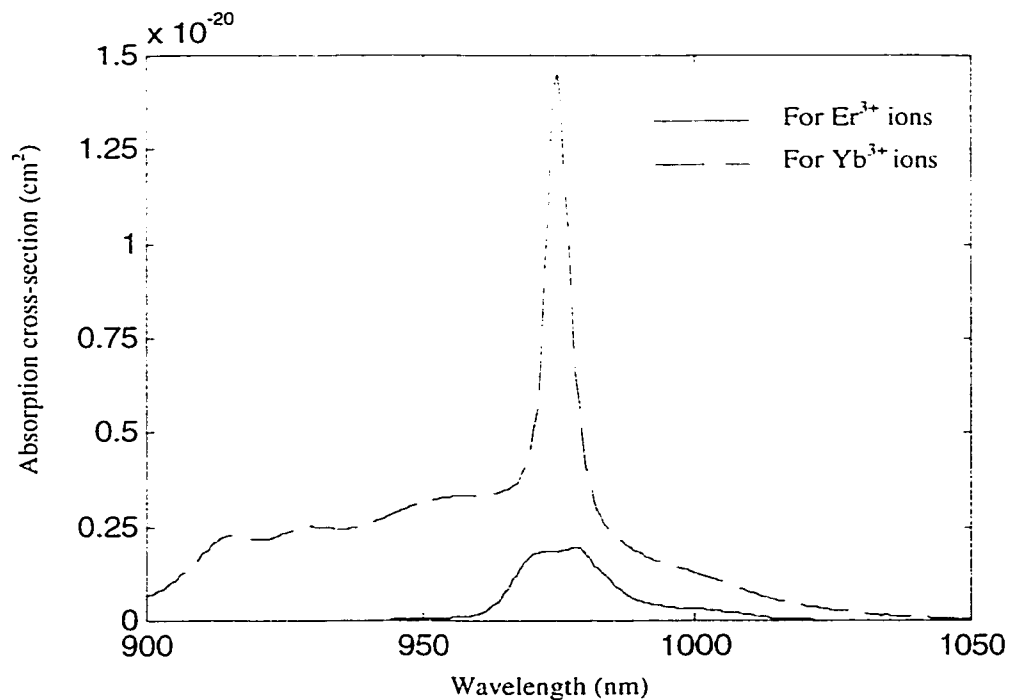
Figure 2.5 The absorption cross-sections for Er^{3+} and Yb^{3+} ions in a commercially available multi-component phosphate glass [37].

This indirect pumping of Er^{3+} ions via the Yb^{3+} ions makes use of some favorable properties of Yb^{3+} ions, listed as follows. Firstly, the ionic radius of Yb^{3+} ion is close to that of Er^{3+} ion, making it possible to surround each Er^{3+} ion with several Yb^{3+} ions. Secondly, since the Yb^{3+} ion has only two energy states, ground and the 980 pump state (within the energy range of interest), it ensures that there is no ion-ion interaction among the Yb^{3+} ions. The most advantageous property is that since the absorption cross-section spectra for the Yb^{3+} ion is higher and wider than that of the Er^{3+} ion, it allows amplification at relatively low pump powers together with a flexibility in choosing pump lasers at wavelengths around 980 nm. As an example, the absorption cross-section spectra for Er^{3+} and Yb^{3+} ions around 980 nm for a multi-component phosphate glass [37] is plotted in Figure 2.5. The optimum signal amplification through an efficient energy transfer process, however, is determined by the concentration levels of Er^{3+} and Yb^{3+} ions, the ratio between them in a given system and the optical properties of the base material [38],[39].

2.4 Amplifier model formulation

The numerical model developed in this work for analyzing the highly concentrated Er/Yb co-doped waveguide amplifier is based on various models presented in references [9],[34],[40]-[42],. A combination of the finite difference method with a Runge-Kutta algorithm is used in modeling the amplifier. A multi-level system with 980 nm pumping is considered. The model takes into account the forward travelling (along with signal propagating direction) ASE noise in the signal band. ASE noise in the pump band is not included in the model. The different energy levels and all the transitions that are relevant to the model are shown in Figure 2.4. Populations in six different energy levels, marked as level 1 up to level 4 for Er and level 5 and level 6 for Yb, are tracked in the simulations. The population in the $^2H_{11/2}$ energy state for Er ions is not taken into account due to very short lifetime and the negligible population densities that exist for that state. It is assumed that the ions are homogeneously distributed, thus the pair-induced upconversion effect is zero. The population densities at different energy levels, N_i, (i=1,2..6) which are functions of time and position can be related to the total ion densities in the medium as

$$N_{Er} = N_1 + N_2 + N_3 + N_4 \qquad (2.8)$$

$$N_{Yb} = N_5 + N_6 \qquad (2.9)$$

where N_{Er} and N_{Yb} are the Er and Yb ion densities respectively. With these two conservation equations, another set of four rate equations that describe the rate at which ions in the energy levels are populated and depleted by absorption, emission, relaxation and ion-ion interactions, can serve to solve for the six unknown population densities. Accordingly, the rate equations for levels 1 to 3 and level 5 can be written as follows

$$\frac{\partial N_1}{\partial t} = -W_{12}N_1 - R_{13}N_1 + A_{21}^R N_2 + W_{21}N_2 + C_{up2}N_2^2 + C_3N_3^2$$
$$- C_{14}N_1N_4 - K_{tr}N_1N_6 \qquad (2.10)$$

$$\frac{\partial N_2}{\partial t} = W_{12}N_1 - A_{21}^R N_2 - W_{21}N_2 + A_{32}N_3 - 2C_{up2}N_2^2 + 2C_{14}N_1N_4 \qquad (2.11)$$

$$\frac{\partial N_3}{\partial t} = R_{13}N_1 - A_{32}N_2 + A_{43}N_4 - 2C_{up3}N_3^2 + K_{tr}N_1N_6$$
$$- R_{ESA}N_3 \qquad (2.12)$$

$$\frac{\partial N_5}{\partial t} = -R_{56}N_5 + A_{65}^R N_6 + R_{65}N_6 + K_{tr}N_1N_6 \qquad (2.13)$$

where W_{ij}, and R_{ij}, represent stimulated transition rates per ion (absorption or emission) at signal and pump wavelengths respectively, occurring from i^{th} to j^{th} level; A_{ij} and A_{ij}^R represent the non-radiative and radiative decay rates per ion respectively, and both are given by $A_{ij} \equiv A^R_{ij} = 1/\tau_{ij}$, τ_{ij} being the lifetime for the ions to decay from i^{th} to j^{th} level; R_{ESA} is the ESA rate occurring at level 3; C_{up2} and C_{up3} are the upconversion coefficients used to model the co-operative upconversion effects in level 2 and level 3 respectively; similarly, C_{14} is the cross-relaxation coefficient for the interaction among ions from level 1 and level 4; and the coefficient, K_{tr}, represents the net or forward energy transfer from Yb ions (in level 6) to Er ion (in level 1). In the steady state regime, the population densities are computed by imposing $\dfrac{\partial N_i}{\partial t} = 0$ (for i=1,2..,6) in the rate Equations.

The stimulated transition rates of signal and pump are given by,

$$R_{13} = \frac{\sigma_{13}(\upsilon_p)}{h\upsilon_p} I_p(\upsilon_p) \qquad (2.14)$$

$$R_{56} = \frac{\sigma_{56}(\upsilon_p)}{h\upsilon_p} I_p(\upsilon_p) \qquad (2.15)$$

$$R_{65} = \frac{\sigma_{65}(\upsilon_p)}{h\upsilon_p} I_p(\upsilon_p) \qquad (2.16)$$

$$R_{ASE} = \frac{\sigma_{ASE}(\upsilon_p)}{h\upsilon_p} I_p(\upsilon_p) \qquad (2.17)$$

$$W_{12} = \frac{\sigma_{12}(\upsilon_s)}{h\upsilon_s} I_s(\upsilon_s) + \sum_{k=1}^{121} I_{ASE+}(\upsilon_k) \frac{\sigma_{12}(\upsilon_k)}{h\upsilon_k} \qquad (2.18)$$

$$W_{21} = \frac{\sigma_{21}(\upsilon_s)}{h\upsilon_s} I_s(\upsilon_s) + \sum_{k=1}^{121} I_{ASE+}(\upsilon_k) \frac{\sigma_{21}(\upsilon_k)}{h\upsilon_k} \qquad (2.19)$$

where υ_p and υ_s are the pump and signal frequencies respectively; h is Planck's constant; I_p, I_s, and I_{ASE+} are the pump, signal and forward travelling ASE intensities respectively; σ_{12}, σ_{13} and σ_{21} are absorption and emission cross-sections for Er^{3+} ions and σ_{56} and σ_{65} are absorption and emission cross-sections for Yb^{3+} ions; and σ_{ESA} represents the ESA cross-section for Er^{3+} ions. For the transition rates W_{21} and W_{12}, the net contribution from ASE noise spectrum in the signal band is also added to the signal induced transitions. ASE noise power is modeled by spectrally resolving the ASE noise band (1470 nm – 1590 nm) into 121 wavelength slots, each of width 1nm.
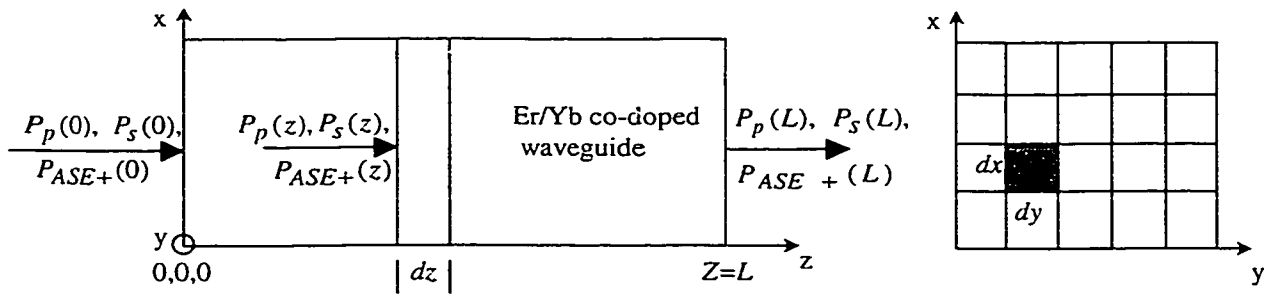
Figure 2.6 Schematic of the waveguide modeled (a) power levels along the waveguide (b) grid formation across the waveguide cross-section.

The evolution of pump (P_p), signal (P_s), and forward-travelling ASE (P_{ASE+}) powers along the waveguide length, as shown in Figure 2.6, can be described by the following differential equations

$$\frac{dP_p(z,\upsilon_p)}{dz} = -[\gamma_p(z,\upsilon_p) + l_p]P_p(z,\upsilon_p) \tag{2.20}$$

$$\frac{dP(z,\upsilon_s)}{dz} = [\gamma_s(z,\upsilon_s) - l_s]P_s(z,\upsilon_s) \tag{2.21}$$

$$\frac{dP_{ASE+}(z,\upsilon_k)}{dz} = [\gamma_{ASE}(z,\upsilon_k) - l_k]P_{ASE+}(z,\upsilon_k)$$
$$+ h\upsilon_k\Delta\upsilon_k\gamma_{21}(z,\upsilon_k) \tag{2.22}$$

The absorption and emission coefficients, γ_p, γ_s, and γ_{ASE} in Equations 2.20- 2.22, are spatial overlap integral expressions and in terms of the normalized pump and signal intensity profiles, $\overline{\psi}_p(x,y)$ and $\overline{\psi}_s(x,y)$, respectively, are given by

$$\gamma_p(z,\upsilon_p) = \iint\limits_{A}\overline{\psi}_p(x,y)[\sigma_{13}(\upsilon_p)N_1(x,y)$$

$$+ (\sigma_{56}(\upsilon_p)N_5(x,y) - \sigma_{65}(\upsilon_p)N_6(x,y))]dxdy \tag{2.23}$$

$$\gamma_s(z,\upsilon_s) = \iint\limits_{A}\overline{\psi}_{s(x,y)}[\sigma_{21}(\upsilon_s)N_2(x,y) - \sigma_{12}(\upsilon_s)N_1(x,y)]dxdy \tag{2.24}$$

$$\gamma_{ASE}(z,\upsilon_k) = \iint\limits_{A}\overline{\psi}_{s(x,y)}[\sigma_{21}(\upsilon_k)N_2(x,y) - \sigma_{12}(\upsilon_k)N_1(x,y)]dxdy \tag{2.25}$$

The signal intensity profile $\overline{\psi}_s(x,y)$ is assumed to coincide for all the ASE fields in the ASE spectrum, i.e., $\overline{\psi}_s(x,y) \equiv \overline{\psi}_k(x,y)$, for $k=$ 1 to 121. However, the emission and absorption cross-sections, which strongly depend on the wavelength, are taken separately in each ASE wavelength slot. The waveguide background losses are represented by l_p, l_s and $l_k(=l_s)$ for pump, signal, and ASE respectively. In Equation 2.22, the second extra term in the right side represents the newly generated ASE noise in each consecutive step along the direction of propagation. A is the cross-sectional area of the active waveguide region and is assumed to be uniform throughout the length of the waveguide.

The relationship among the intensity profiles ($I(x, y, z)$), power levels ($P(z)$) and the normalized intensity profiles $\overline{\psi}(x, y)$ for pump, signal and ASE are given by [34]

$$I(x, y, z) = P(z)\overline{\psi}(x, y) \tag{2.26}$$

2.5 Method of solution

A code in Matlab was written for running simulations of the numerical model developed in the previous section. The following parameters are assumed to be known and are taken as the input data to the model: waveguide parameters:- dimensions, index profile, rare-earth concentration levels, and the waveguide background losses (A, L, n_g, N_{Er}, N_{Yb}, l_s, and l_p); the material-dependent optical properties:- absorption and emission cross-sections for both Er and Yb ions at all interested wavelengths, lifetime for ions at different energy levels, and the coefficients for upconversion and cross-relaxation (σ, τ, and C); and the power levels at the input end of the waveguide ($P_s(0), P_p(0)$, and $P_{ASE}(0)$). For the given waveguide structure the normalized intensity profiles ($\overline{\psi}(x, y)$) at pump and signal wavelengths are generated as discussed in Section 2.1. In the case of a uniform waveguide, where the waveguide parameters remain unchanged along the length of the waveguide, the normalized intensity profiles, $\overline{\psi}(x, y)$, are z-independent.

Initially, at the input end of the waveguide the local intensity profiles are calculated using Equation 2.26. Then, the steady-state population density profiles ($N_1(x, y)$ to $N_6(x, y)$ in each finite grid are found from Equations 2.8 through 2.13 using a Newton-Raphson method [9]. These values are then substituted into Equations 2.23 – 2.25 and the propagation coefficients are obtained by integrating the contribution from all finite grids formed across the waveguide cross-section (Figure 2.6). The changes in optical powers over a finite distance, dz, are then calculated from the Equations 2.20, 2.21, and 2.22. Now the power levels at a finite distance dz from the input end of the waveguide are known and the set of calculations is repeated to update the power levels as the signals travel by the next finite distance, dz, along the waveguide. This procedure is continued until the signals reach the output end of the waveguide. The net signal gain, pump absorption and the gain coefficient of the waveguide amplifier are calculated as

21

$$\text{Net Signal Gain} = 10Log_{10}\left[\frac{P_s(L)}{P_s(0)}\right] \qquad \text{(dB)} \qquad \text{(2.28)}$$

$$\text{Net Pump Absorption} = 10Log_{10}\left[\frac{P_p(L)}{P_p(0)}\right] \qquad \text{(dB)} \qquad \text{(2.29)}$$

$$\text{Gain Coefficient} = \frac{\text{Net Signal Gain}}{L} \qquad \text{(dB/cm)} \qquad \text{(2.30)}$$

where L is the length of the amplifier.

2.6 Applications and discussions

2.6.1 Validation of the model for Er-doped waveguide amplifiers

The amplifier model developed as described above was firstly validated for an Er-doped waveguide amplifier reported in [10],[11] by comparing the simulation results obtained with the experimental results reported in the reference. A strip-loaded wave-guide structure was fabricated by rf sputter deposition techniques using a multi-component phosphate glass. The amplifier net gain of 4.1 dB was achieved in a 1 cm waveguide. The cross-section and the refractive indices of the waveguide structure are shown in Figure 2.7.
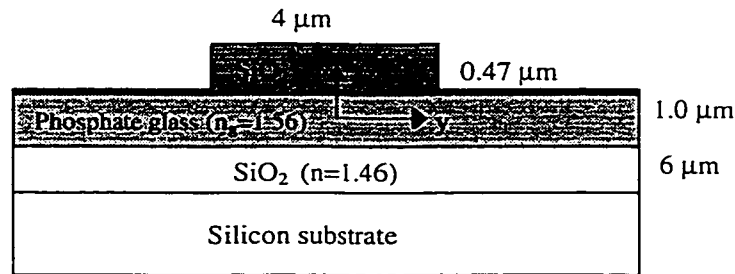
Figure 2.7 Cross-section of the strip-loaded waveguide. Dimensions are not to scale.

The waveguide is single moded at both pump and signal wavelengths. Figure 2.8 shows the TE field contours for both signal and pump across the waveguide cross-section. The normalized intensity variation across the center of the (Er-doped) active region is shown in Figure 2.9. As seen in both plots, Figure 2.8 and 2.9, the modes are tightly confined within the core layer and there is a good overlap between the pump and signal (pump intensity exceeds the signal intensity across the core region).
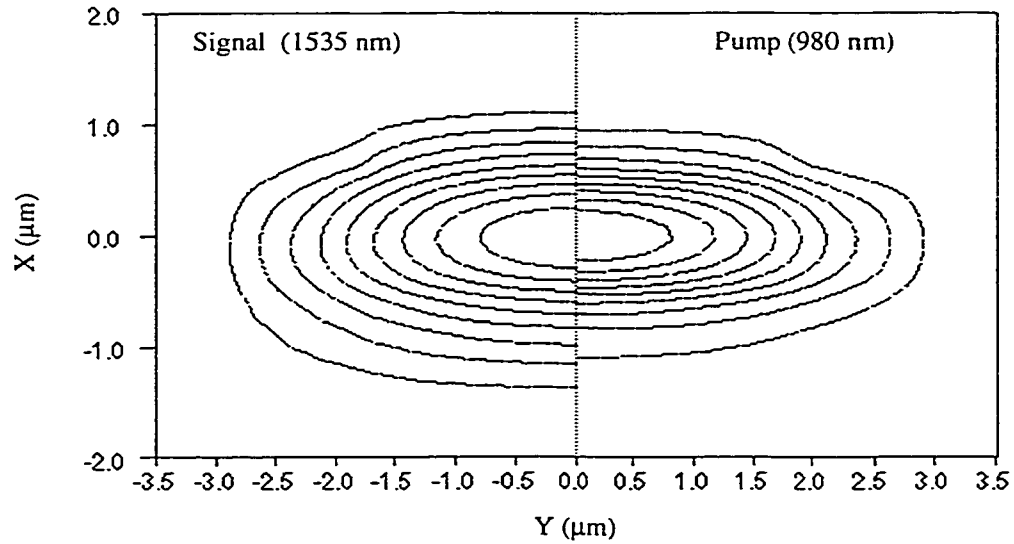
Figure 2.8 Electric field (TE) contours at signal (1535 nm, on the left) and pump (980 nm, on the right) wavelengths for the strip-loaded waveguide shown in Figure 2.6. The contours represent 90 % to 10 % of the peak amplitude.
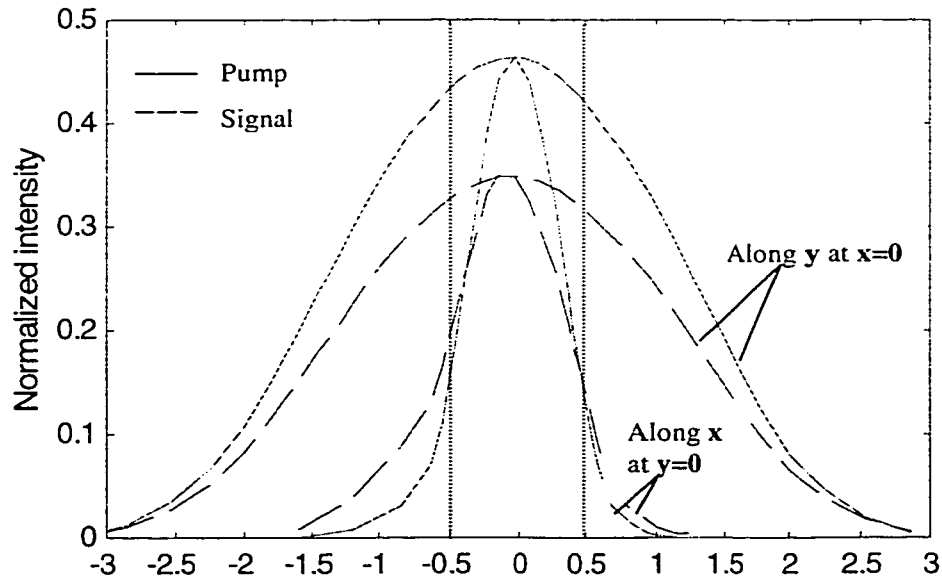
Figure 2.9 Normalized pump and signal intensity profiles along the center of the core of the strip-loaded waveguide.

The amplifier parameters used for the simulations are listed in Table 2.1, as reported in [10],[11]. The coefficients C_{up3} and C_{14} were assumed to be in the same order and close to C_{up2}. For the calculation of ASE power, the unknown emission and

absorption cross-section values over the ASE band for the glass used were estimated from the known values of another similar multi-component phosphate glass [37]. The spectral shape and peak wavelengths were found to be similar for both glasses and the cross-section data for the glass in [11] were calculated by scaling the normalized spectra of [37] (shown in Figure 2.10) to the peak values reported in [11]. The length of the amplifier was 1 cm. The comparison was performed for the net signal gain as a function of pump power in the waveguide input. Initially, the ESA effect, which was not reported as observed in the experiment, was neglected in the calculations. The input signal power was taken as 0.5 μW.

Table 2.1 Parameters used for the simulations on strip-loaded waveguide [10],[11].

Parameter	Value
Er ion density (m^{-3})	5.3×10^{26}
Wavelengths (nm): signal/pump	1535 / 980
Lifetime (ms): metastable state ($^4I_{13/2}$)	4
Lifetime (μs): $^4I_{11/2}$ and $^4I_{9/2}$	2.7 *
Er^{3+} absorption cross-sections (m^2): $\sigma_{12(\lambda)}$	5.4×10^{-25} (1535 nm)
Er^{3+} absorption cross-sections (m^2): $\sigma_{13(\lambda)}$	2.2×10^{-25} (980 nm)
Er^{3+} emission cross-sections (m^2): $\sigma_{21(\lambda)}$	5.4×10^{-25} (1535nm)
Upconversion coefficient (m^3/s): C_{up2}	$2 \pm 0.5 \times 10^{-24}$
Waveguide loss (dB/cm): $l_s = l_p$	0.9
Upconversion coefficient (m^3/s): C_{up3}/ C_{14}	2.0×10^{-24}/ 2.0×10^{-24}

*Estimate based on reported values in similar phosphate glass [7].

Figure 2.11 shows both the simulated net signal gain obtained for two values of C_{up2}, 2.25×10^{-24} m^3/s (solid line) and 2.5×10^{-24} m^3/s (dashed line), and the experimental data (circles) [11]. As seen, a good agreement between the model presented in this thesis and the measured data [11] is obtained. The numerical model best fit the experimental values for the upconversion coefficient (C_{up2}) values in the range of $2.25 \times 10^{-24} < C_{up2} < 2.5 \times 10^{-24}$. It also reveals that even a small increase in C_{up2} causes a significant reduction in the amplifier gain. However, it was noticed that similar variations on upconversion coefficients C_{up3} and C_{14} did not show any significant changes on the signal gain. This

feature can be explained by the following two reasons: (1) the population densities in the metastable state (level 2) are much higher than in the other states (level 3 and level 4) due to the long lifetime in level 2; (2) the removal of (two) ions from level 2 through the upconversion process (modeled by (C_{up2})), directly affects the emission rate at the signal wavelength and thereby influences the amplifier gain considerably.
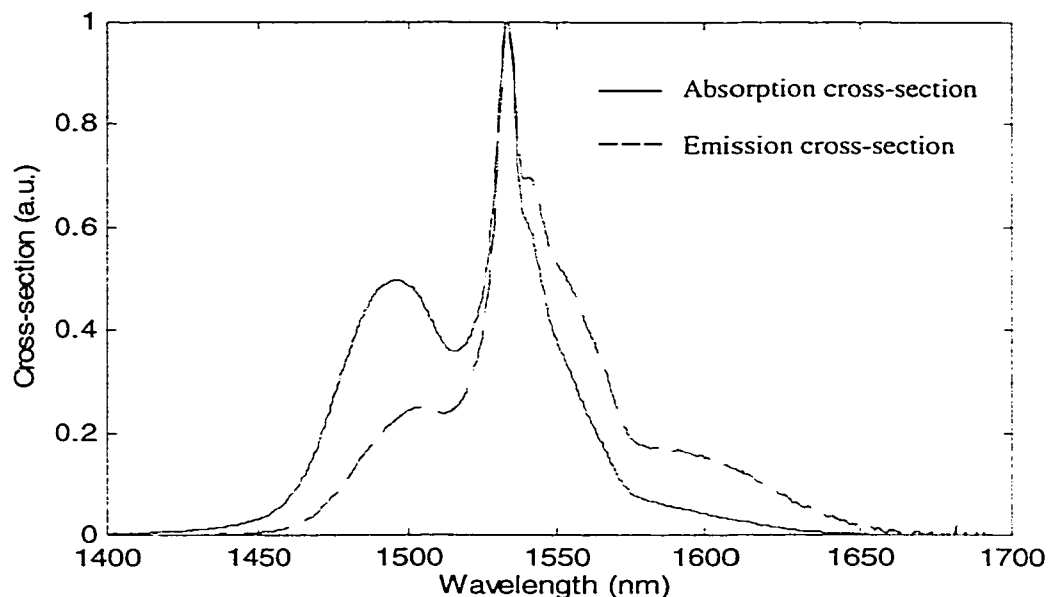
Figure 2.10 Absorption and emission cross-section spectra (normalized to peak values) for Er ions in a muliticomponent phosphate glass, designated as IOG-1 [37]. Peak wavelength for both absorption and emission is 1534.6 nm.
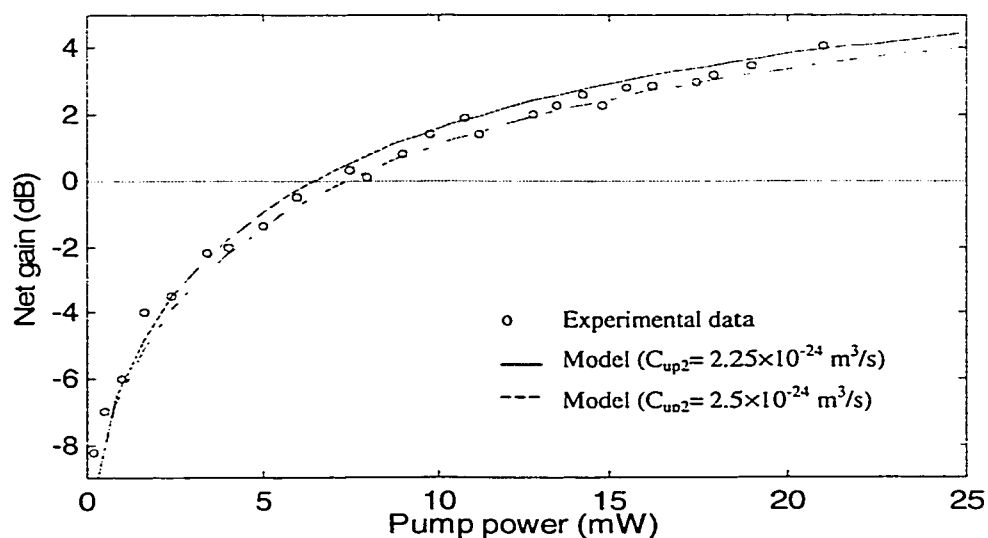
Figure 2.11 Gain versus pump power for the strip-loaded waveguide. Calculated results, using the model developed in this thesis, are shown by lines. The measured values [11] are shown by circles.

Next the impact of ESA for this amplifier was studied. To model ESA, the knowledge of the ESA absorption cross-section for the glass was required. In the absence of any experimentally measured data on ESA cross-section for phosphate-based glasses around 980 nm found in the literature, some values in the same order as of ground state absorption at 980 nm (σ_{13}), were used to calculate the amplifier gain. No significant reduction in amplifier gain was observed even at high pump powers. Both curves, with and without ESA, coincide as shown in Figure 2.12. The short lifetime for Er^{3+} ions in the pump state, could have possibly eliminated accumulation and any removal of ions from the pump state through the ESA effect.
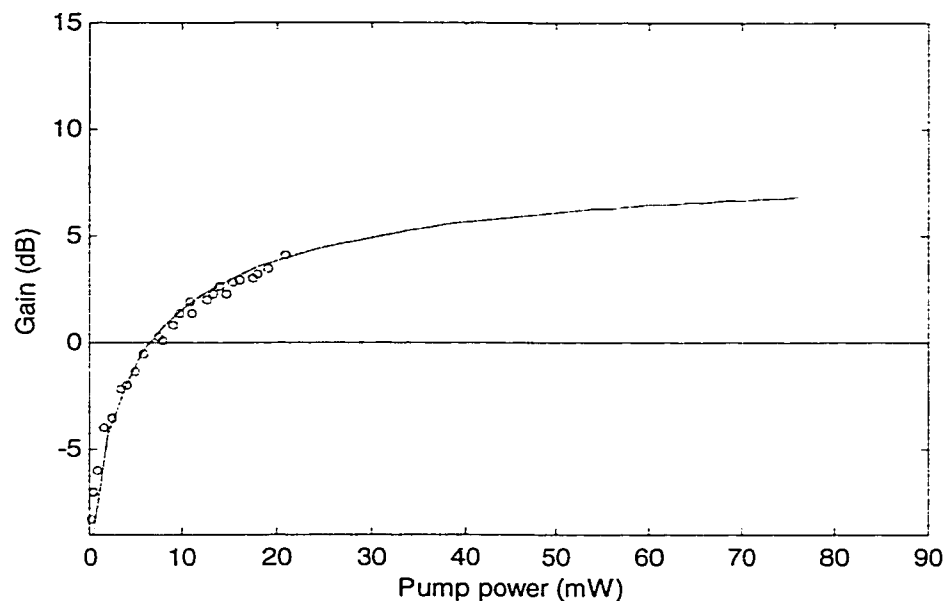
Figure 2.12 Gain versus pump power, calculated with and without the ESA effect. Both curves coincide as shown by the line. Circles represent the measured data [11]; Length = 1cm, Input signal power =0.5 μW.

Up to now, this is the highest amplifier gain (per cm) demonstrated in Er-doped planar waveguide amplifiers. The obvious reasons are high Er doping level, tight mode confinement inside the core because of the large index difference between the core and claddings, and a low upconversion coefficient (C_{up2}) realized in this multi-component phosphate glass compared to those from other materials (e.g. for silica based glass, C_{up2} > 3.0×10^{-24} m^3/s [3]). Moreover, the low upconversion effect helps in achieving high gain at relatively low pump powers.
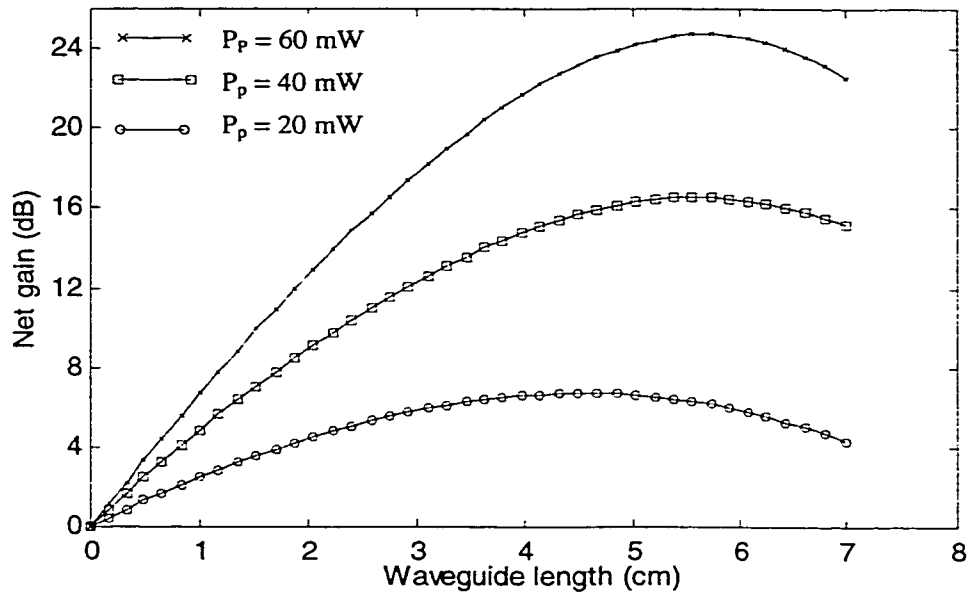
Figure 2.13 Gain versus waveguide length for the strip-loaded waveguide, calculated at different pump powers.

The signal gain dependence on the waveguide length was examined for the same waveguide structure at different pump powers (P_p), while all other parameters were kept fixed. Figure 2.13 shows the simulation results obtained for pump powers 20, 40, and 60 mW. For a fixed input pump power the gain increases linearly with the waveguide length and beyond a certain length gain starts to decrease. This behavior can be explained as follows. The pump power is being absorbed by the ground state Er ions as it travels along the waveguide. When the pump power level falls below a threshold value the population inversion can't be maintained beyond that point in the waveguide and the signal photons are absorbed by the ground state Er ions. This effect eventually reduces the signal intensity at the output of the waveguide. Therefore, there exists an optimum length for a given pump power to realize the maximum gain in the amplifying device. However, the maximum available gain can be further increased using longer devices together with higher input pump powers.

2.6.2 Validation of the model for Er/Yb co-doped waveguide.

There have been reports describing the successful realization of Er/Yb co-doped waveguide amplifiers in the fast few years [6]-[8]. In all these works, the waveguides were fabricated using ion-exchange (or diffusion) techniques and as a result the waveguides formed had graded index profiles. However, little information on these waveguide structures is available in the literature to generate the field profiles which are needed to model the amplifiers. To date, there has been no published experimental work available on Er/Yb co-doped amplifiers with step index profiles or with discrete waveguide boundaries. The model developed in this thesis was then instead verified with some theoretical results presented in [41]. The simulation results generated were found in good agreement with the theoretical results reported with model in [41] and they are not repeated here. Some of the analysis on the Er/Yb co-doped amplifier, discussed in the following section, will still reveal similar trends with those found in [41].

2.6.3 Theoretical analysis of Er-doped and Er/Yb co-doped waveguide amplifiers characteristics

The numerical model, developed and verified, was then used in studying the dependence of the amplifier characteristics in terms of various device parameters such as rare-earth concentration levels, device dimensions, pump and signal powers, and material dependent parameters. A strip-loaded waveguide structure, shown in Figure 2.14, was considered for the purpose of this analysis. For a given refractive index n_g, the waveguide dimensions, w, h, and d, were selected such that the structure is single-moded at both signal and pump wavelengths.
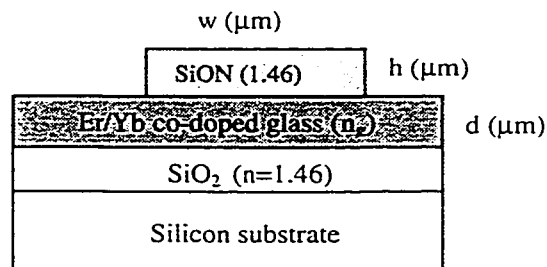
Figure 2.14 Waveguide structure used for the analysis of Er/Yb co-doped waveguide amplifier.

The study was carried out with a commercially available Er/Yb co-doped phosphate-glass-based material for which the relevant material parameters (absorption and emission cross-section spectra for Er and Yb ion around both pump and signal wavelengths) were known, as obtained from the supplier [37]. The electric field contours generated for this waveguide structure are plotted as shown in Figure 2.15. The dimensions were taken as 1.6, 1.0, and 9.0 for d, h, and w respectively. The normalized intensities along the centerlines at pump and signal wavelengths are shown in Figure 2.16. Within the core area, the normalized pump intensity exceeds that of signal intensity all along in the y direction but in the direction of x, the normalized pump intensity exceeds that of signal approximately only up to half way towards the core-cladding boundaries. As the index difference between the core and cladding layers gets smaller, the limiting thickness for the fundamental mode operation of the core layer increases and the mode profiles for pump and signal spread out more and results in a weaker overlap between them. The effect of the pump intensity being too small for significant population inversion is that signal photons will be absorbed by the ground state Er ions. To overcome this, more pump power is required.
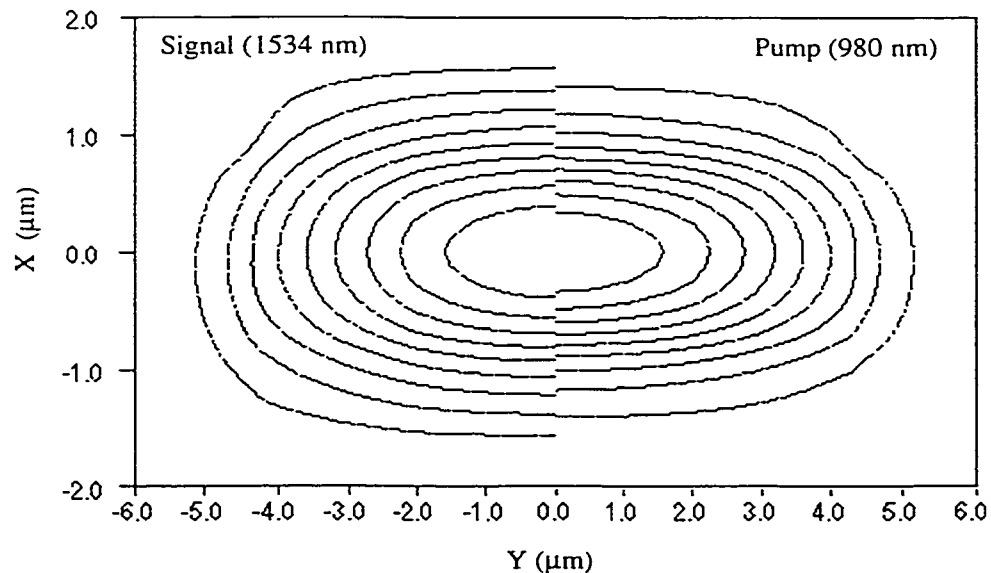
Figure 2.15 Electric field (TE) contours at signal (1535 nm, on the left) and pump (980 nm, on the right) wavelengths for the strip-loaded waveguide shown in Figure 2.14. The contours represent 90 % to 10 % of the peak amplitude.
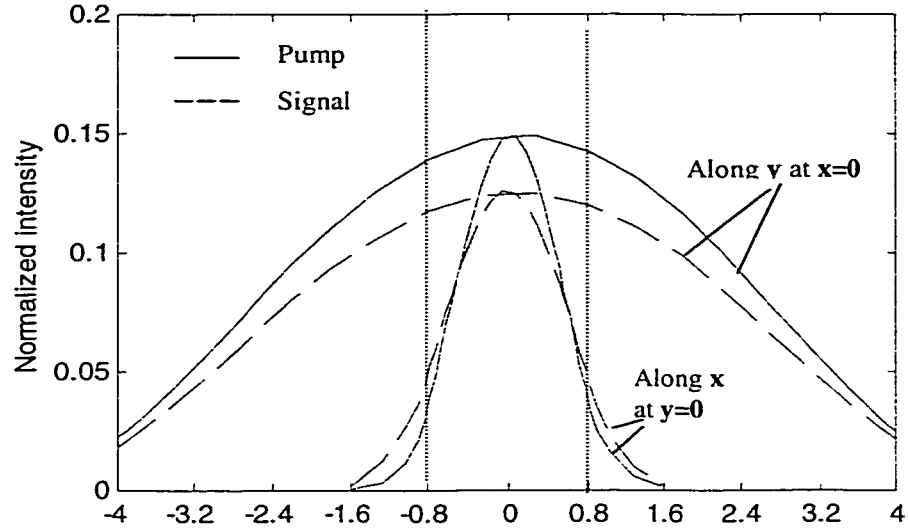
Figure 2.16 Normalized pump and signal intensity profiles along the center of the core of the strip-loaded waveguide shown in 2.14.

Table 2.2 Parameters used to model the Er/Yb co-doped waveguide amplifier.

Parameter	Value
Refractive index (n_g)	1.515
Dimensions (μm): w/d/h	9/1.6/1
Ion densities (m^{-3}): Er / Yb	Varied
Wavelengths (nm): signal/pump	1534/ 980
Lifetime (ms): metastable state ($^4I_{13/2}$)	8
Lifetime (μs): $^4I_{11/2}$	2.7* [7]
Lifetime (ns): $^4I_{9/2}$	1* [6]
Lifetime (ms): $^2F_{7/2}$	1.4* [7]
Er^{3+} absorption cross-sections (m^2): $\sigma_{12(\lambda)}$	6.70×10^{-25} (1534 nm)
Er^{3+} absorption cross-sections (m^2): $\sigma_{13(\lambda)}$	1.87×10^{-25} (980 nm)
Er^{3+} emission cross-sections (m^2): $\sigma_{21(\lambda)}$	6.64×10^{-25} (1534 nm)
Yb^{3+} absorption cross-sections (m^2): $\sigma_{56(\lambda)}$	4.52×10^{-25} (980 nm)
Yb^{3+} emission cross-sections (m^2): $\sigma_{65(\lambda)}$	6.62×10^{-25} (980 nm)
Upconversion coefficient (m^3/s): C_{up2}	1.0×10^{-23} * [6],[7]
Waveguide loss (dB/cm)	0.8* [9]
Upconversion coefficient (m^3/s): C_{up3}/C_{14}	2.5×10^{-24}/ 2.5×10^{-24} * [7]
Cross-relaxation coefficient (m^3/s): C_{cr56}	1.0×10^{-22} * [6],[7]

*Estimate based on the reported values for similar glasses

The parameters and the values that were taken as the input data are shown in Table 2.2. Gain characteristics of the amplifier were first examined as a function of Er concentration. The length of the amplifier was taken as 1 cm and the input powers for pump and signal were taken as 100 mW and 1 μW respectively. Figure 2.17 shows the gain curves obtained at different concentration levels for Yb. In all cases gain improves with increasing Er concentration except for the purely Er-doped waveguide (N_{Yb}=0), where the gain starts to decrease above a certain concentration level due to the upconversion effect, C_{up}. For the Er-doped waveguide the inefficiency caused by the upconversion effect at higher concentration levels can be clearly seen by a comparison of curves plotted with and without taking the upconversion into effect. But in the Er/Yb co-doped waveguides this negative effect at high Er concentrations is reduced by the efficient energy transfer from Yb to Er ions [41]. Moreover, the gain is further improved for increasing Yb concentrations. The inclusion of the ESA effect, modeled with an ESA absorption cross-section equal that of ground state absorption, again did not show any change in gain for all cases as shown in Figure 2.17.
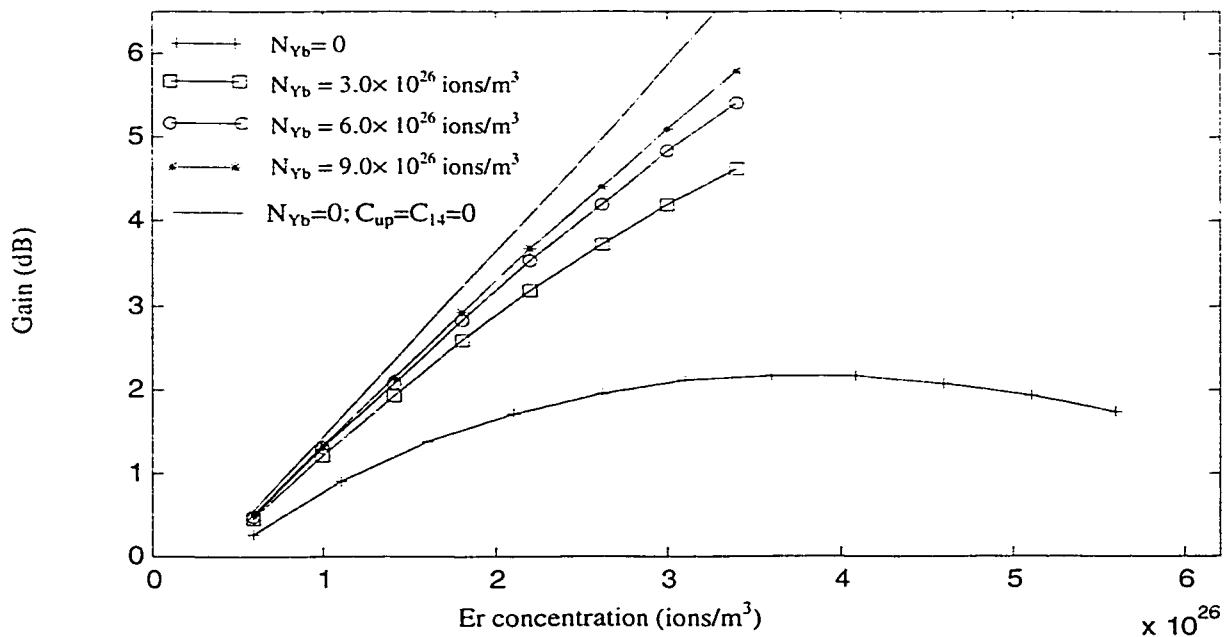
Figure 2.17 Signal gain versus Er concentration (L =1 cm, $P_p(0)$=100 mW, $P_s(0)$=1 μW).
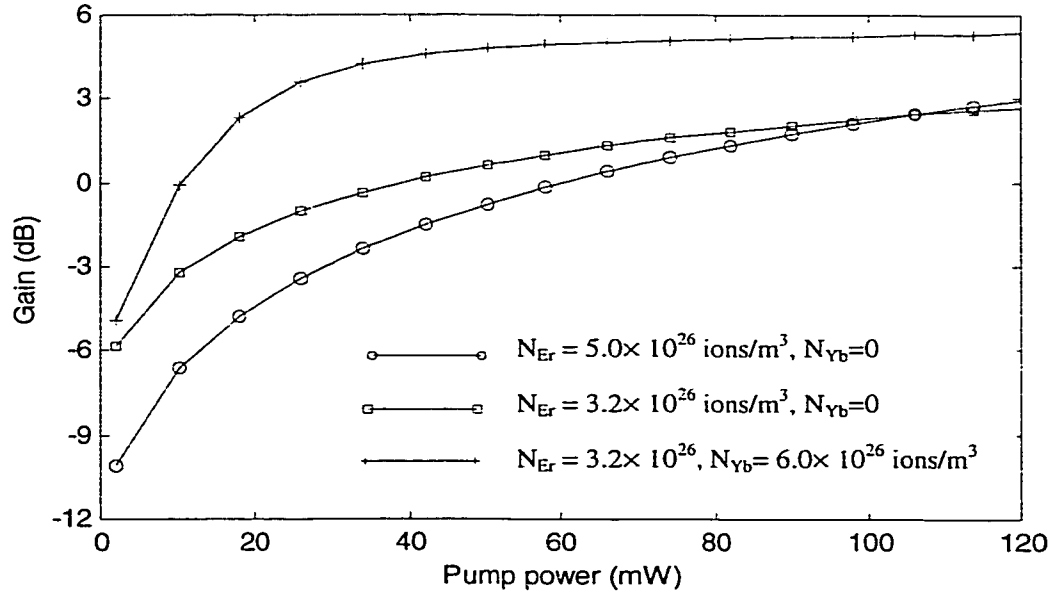
Figure 2.18 Gain versus pump power (L =1 cm, $P_s(0)$=1 μW).

Figure 2.18 shows the gain as a function of input pump power and different concentration levels for Er and Yb. For the co-doped waveguide the signal transparency and the maximum gain (saturated gain) are achieved at relatively low pump powers. As for the Er-doped waveguides, higher pump powers are required to overcome or compete with the upconversion effect and to maintain the population inversion and signal amplification.

The evolution of pump and signal powers was investigated for both Er-doped and Er/Yb co-doped waveguides. Figures 2.19 and 2.20 show the pump and signal powers, respectively, as a function of waveguide length. The pump absorption for the Er-doped waveguide is relatively low (~1.7 dB/cm) and remains uniform throughout the waveguide length of 4 cm. But for the co-doped waveguide the pump absorption is higher due to the additional absorption by the Yb ions. The absorption rate is nearly constant (3 dB/cm) for the first 2 cm and afterwards it increases gradually to ~ 13 dB/cm beyond 3.2 cm in length. The signal power improves slowly over the waveguide length for the Er-doped waveguide. Due to the efficient energy transfer from Yb to Er the co-doped waveguide shows a higher signal enhancement rate. However, the enhancement rate starts to reduce slightly at 2 cm and beyond 3.2 cm signal absorption is incurred instead and the power level decreases. It can be observed that the peak signal power coincides with the big

change in slope of the pump power, at about 6 mW. Below this power level, the pump energy is not large enough for population inversion. As a result, signal absorption is realized in the downstream portion of the amplifier, resulting in signal loss rather than gain in that region. Therefore, treating the waveguide length as a variable and all other parameters are fixed as given above, the amplifier gain is optimized at a waveguide length of 3.2 cm.
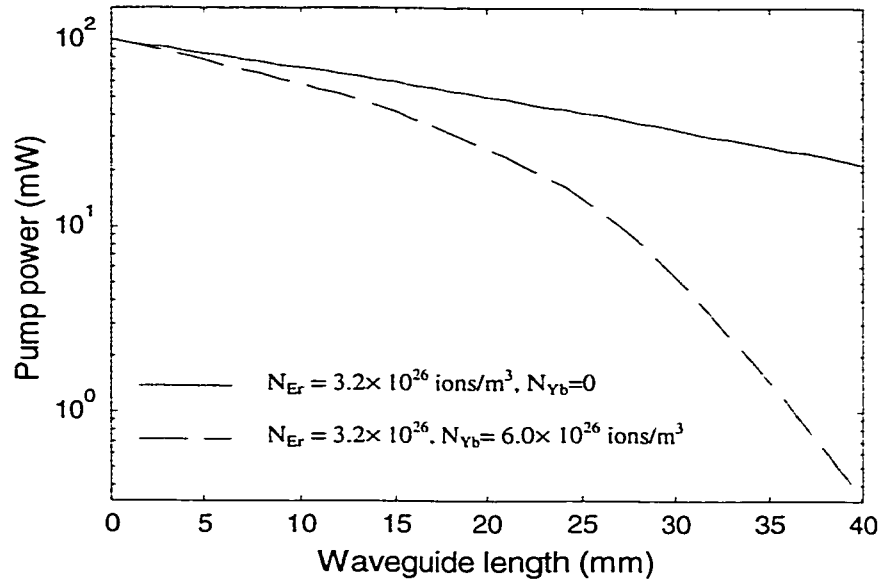
Figure 2.19 Pump power versus waveguide length ($P_p(0)$=100 mW, $P_s(0)$=1 μm).
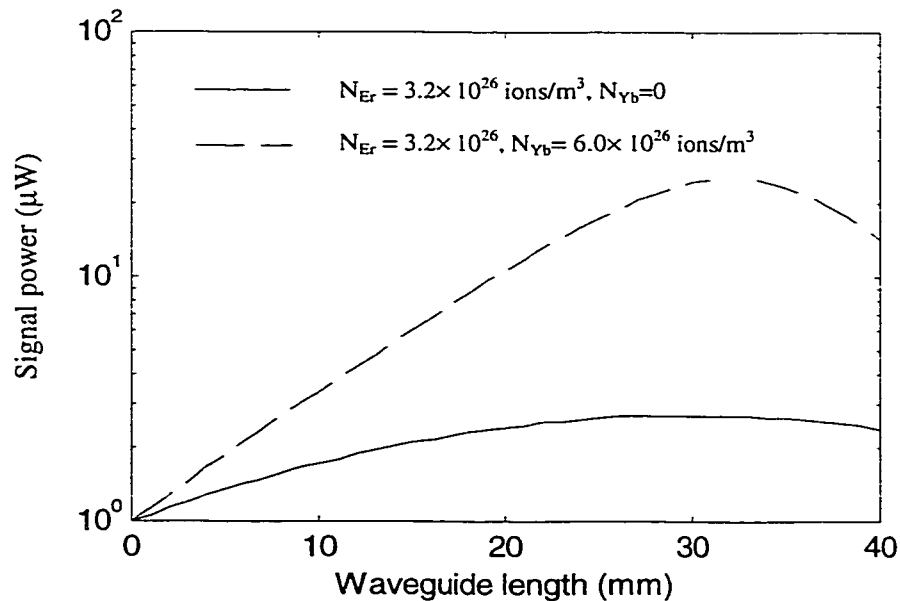
Figure 2.20 Signal power versus waveguide length ($P_p(0)$=100 mW, $P_s(0)$=1 μm).

Figure 2.21 shows the amplifier gain as a function of signal wavelength. The pump power and the pump wavelength were taken as 100 mW and 980 nm respectively. The maximum gain of 5.5 dB (per cm) is achieved at the peak emission wavelength for Er ions at 1534 nm. The wavelength range for the Full Width Half Maximum (FWHM) is 26 nm (1528 - 1554 nm). The shape of the gain curve exactly replicates the emission cross-section spectra for Er ions around the signal wavelength (Figure 2.10). As can be seen in Equation 2.24, the gain coefficient scales with the factor $(\sigma_{21}N_2 - \sigma_{12}N_1)$. However, optimum population inversion is realized ($N_2 \gg N_1$) in the gain region. So the coefficient is dominated by the Er emission cross-section.
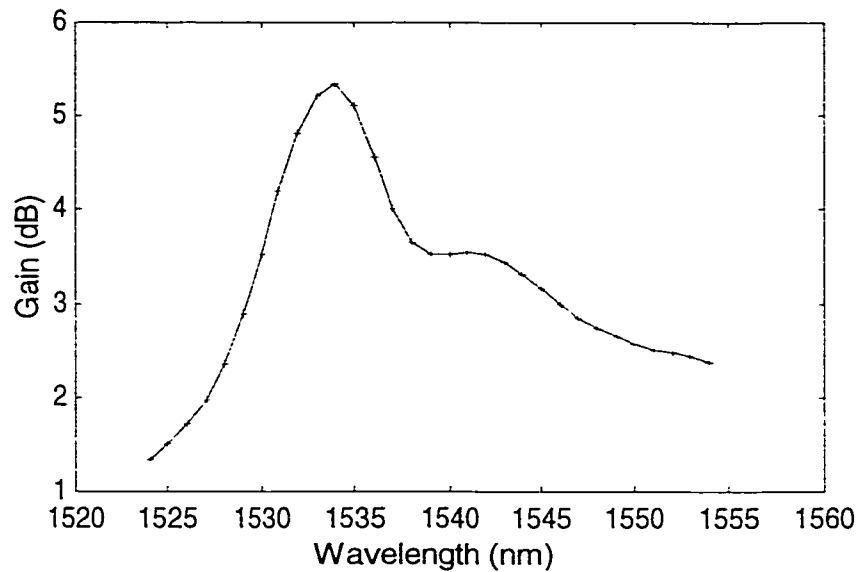
Figure 2.21 Gain as a function of signal wavelength ($P_p(0)$ =100 mW, Length=1 cm, pump wavelength = 980 nm, N_{Er} = 3.2× 10^{26}, N_{Yb}= 6.0× 10^{26} ions/m^3).

Figure 2.22 shows the ASE noise spectrum calculated at the peak gain (signal wavelength of 1534 nm) for the Er/Yb co-doped amplifier at the optimized length of 3.2 cm (Figure 2.20). The total noise power under the spectrum amounts to 7.5 μW. In practical applications, narrow band optical filters are generally used to remove the background noise power as much as possible. However, the noise power that resides within the signal bandwidth cannot be removed with such filters. The in-band (in 1nm width) Signal-to-Noise power Ratio (SNR) for this amplifier is 17.1 dB. Similar to the

gain spectrum, the ASE spectrum resembles the shape of the emission cross-section spectra for Er ions.
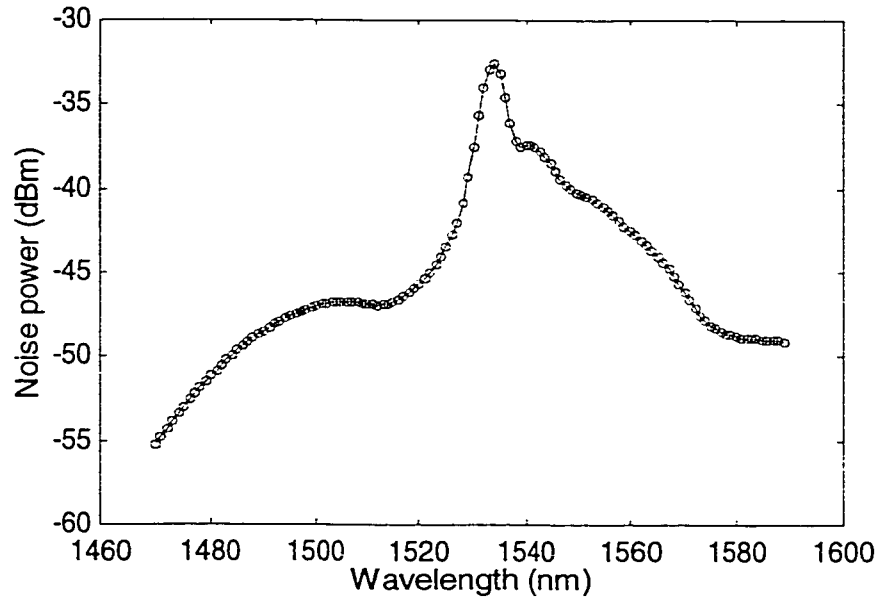
Figure 2.22 ASE noise power as a function of signal wavelength (L= 3.2 cm, $P_p(0)$=100 mW, $P_s(0)$= 1 μW, N_{Er} = 3.2× 10^{26}, N_{Yb}= 6.0× 10^{26} ions/m³).
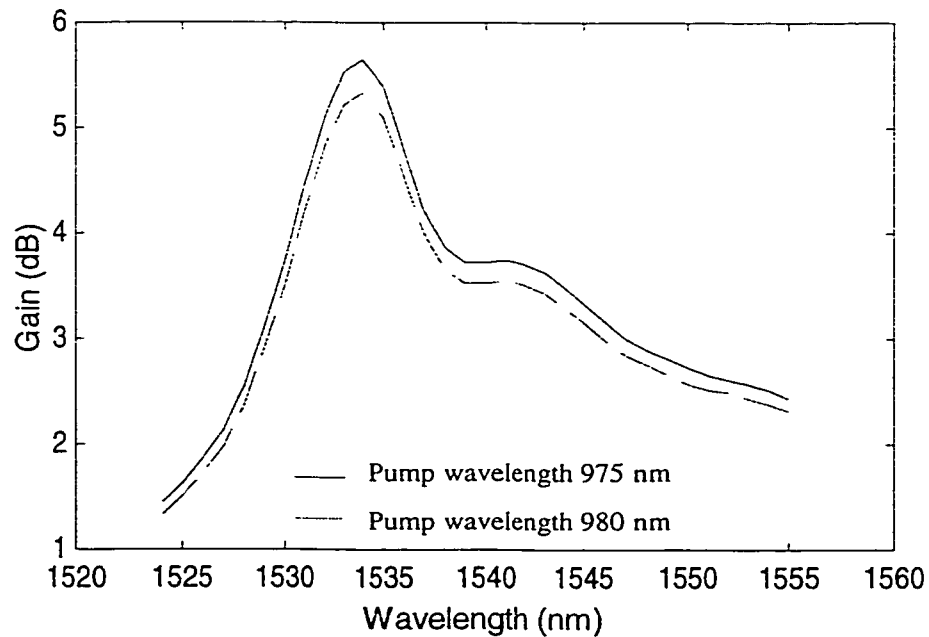
Figure 2.23 Gain as a function of signal wavelength, calculated at peak absorption wavelength of Yb ions, at 975 nm (solid line) and compared with that obtained at 980 nm (dashed line) ($P_p(0)$ =100 mW, Length=1 cm, N_{Er} = 3.2× 10^{26}, N_{Yb}= 6.0× 10^{26} ions/m³).

The Er/Yb co-doped amplifier gain can be improved by pumping it at the peak absorption wavelength for Yb ions, at 975 nm (Figure 2.5). Figure 2.23 shows the amplifier gain calculated at the pump wavelength of 975 nm (solid line), along with the gain obtained at pump wavelength of 980 nm (dashed line). Approximately 0.4 dB of gain improvement is obtained at the peak emission wavelength for this 1 cm waveguide.
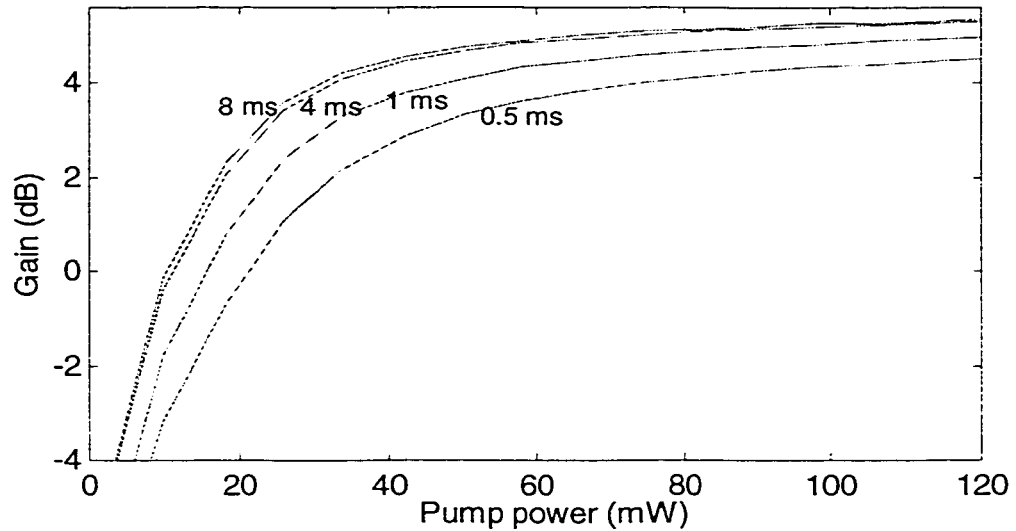
Figure 2.24 Gain versus pump power and lifetime, τ_{21} (Length=1 cm, $N_{Er} = 3.2\times 10^{26}$, $N_{Yb}= 6.0\times 10^{26}$ ions/m^3).

The dependence of the lifetime for Er ions in the metastable state was investigated for the Er/Yb co-doped waveguide amplifier. Figure 2.24 shows the amplifier gain curves as function of pump power obtained at different values of lifetime, τ_{21} (8, 4, 1, and 0.5 ms). As the lifetime drops below 4 ms the reduction in the amplifier gain is noticeable and around 1 dB decrease is observed when the lifetime drops down to 0.5 ms.

Selection of host for Er^{3+} ions and characterization of the bulk glass

3.1 Introduction

Following the successful development of Erbium Doped Fiber Amplifiers (EDFAs), much attention has been given to developing planar waveguide amplifiers to function as loss-compensating element in optical integrated circuits. Over past the decade, several materials have been explored in fabricating waveguide amplifiers using various thin-film technologies. In some cases, reasonable optical gain has been produced in waveguides a few centimeters long (1.0 - 4.1 dB/cm [2],[11],[12]).

It may seem that the concept used in developing EDFAs can be simply transferred to the design of waveguide amplifiers. However, in designing EDFAs, since the length of the amplifier for a given gain is not a critical issue, a good balance between the concentration level of Er^{3+} ions and the fiber length can be maintained. But for an integrated optical amplifier, the device dimensions of a waveguide amplifier need to be compatible with the size of an optical integrated circuit. This requirement necessitates much higher concentration levels of Er ions in the waveguide to realize a reasonable amount of gain. However, at higher concentration levels, the luminescence is quenched by unwanted ion-ion interactions between the neighboring Er^{3+} ions. The extent of the interactions among the ions is mainly related to the material properties of the host glass. Therefore, choosing host materials that dissolve high doping levels of Er ions with even distribution is of prime importance for the successful realization of integrated optical amplifiers.

So far, a wide variety of host materials have been tested for fabricating waveguide amplifiers, including glasses (oxides: pure silica [3], soda-lime silicate glass [5], aluminosilicate glass [12], phosphosilicate glass [3], and multi-component phosphate glass [2],[11], and sulfides: Chalcogenide glass [13],[14]), ceramics (Al$_2$O$_3$, Y$_2$O$_3$ and LiNbO$_3$ [3], and polymers [15]. Silicate and phosphate based multi-component oxide glasses are by far the most widely used materials for developing waveguide amplifiers. In fact, silica glass, being an excellent material for optical fiber amplifiers, has a serious drawback for waveguide amplifiers due to fluorescence quenching at high doping levels

[16],[27]. This limits the Er concentration levels and the total gain achievable in a short amplifier.

Recently, good results have been produced in making lasers and amplifiers using multi-component phosphate glasses [2],[7],[10]. The reason for this is that phosphate glasses, compared to other glass hosts, permit much higher concentration of dopants with minimal effect of ion-clustering and also provide better optical properties such as long lifetime for Er^{3+} ions in the metastable state, and higher emission cross-sections at wavelengths near 1550 nm.

Based on this literature study, phosphate glass was chosen as the host material in this work. After a survey of commercially available laser glasses, Schott Glass Technologies Inc. [37] was identified as a supplier of phosphate laser glasses with any specified dopant levels for Er and Yb ions. Two different glasses, namely stock and custom manufactured glass samples, were obtained from Schott for the purpose of this work. In this chapter, the characterization experiments and the results obtained on the custom melt sample are presented in detail and the results obtained on the stock glass sample are given in summarized from.

3.2 Characterization of Er/Yb codoped IOG-1 phosphate (custom) glass

A set of custom made Er and Yb co-doped glass disks, designated as IOG-1 was purchased form Schott Glass Technologies Inc. for the fabrication of waveguide amplifiers. IOG-1 is a series of multi-component phosphate laser glasses designed for making waveguide lasers and amplifiers. Schott prepared 3" diameter glass disks with thickness of 1 mm and 2 mm, from a custom melt with specified concentration levels of Erbium (3.2×10^{26} ions/m^3) and Ytterbium (6.0×10^{26} ions/m^3). The refractive index of the bulk glass was given as 1.5212 and the density was specified as 2.74 g/cm^3. The exact chemical composition of the glass was not provided by the supplier.

3.2.1 Chemical analysis

In order to identify different elements in the glass, a chemical analysis was carried out using x-ray Energy Dispersive X-ray analysis (EDX), a widely used non-destructive

analytical technique. The EDX system, interfaced with a Scanning Electron Microscope (SEM), uses a beam of focused electrons at energy levels ranging from 10 to 30 KeV to excite characteristic x-rays from a small area of a sample being examined. A Si detector attached to the SEM column converts the intensities of the emitted x-rays into voltage pulses, where the amplitude of the pulses are proportional to the incident x-ray (photon) energy, allowing one to characterize the constituent elements in the sample. Although the exact percentages could not be obtained due to the limited resolution of Si photodetector (~ 150 eV), the EDX analysis identified the presence of P, Er, Yb, Al and Na ions in the glass sample.

To obtain a quantitative analysis, another accessible technique called Electron Microprobe Analysis (EMP) was tried. EMP uses a Wavelength Dispersive System (WDS) detection, rather than energy dispersion, with a resolution of 5eV. Similar to EDX, EMP utilizes electrons to excite X-rays from a small area of the sample. However, the resulting X-rays are diffracted by crystals before impinging on the Si detector. The composition of the unknown sample is determined by a comparison with X-ray intensities from materials with known compositions (standards). The sample is first coated with a thin layer (~250 $\overset{\circ}{A}$) of pure carbon to bleed off the electrical charge produced by the incident electron beam. Carbon is chosen because it does not absorb most X-rays of interest and is not itself an element of interest. For an applied accelerating voltage of 15 kV, the composition analysis (for oxides) obtained in Wt % is listed in Table 3.1. From this composition analysis the corresponding Er^{3+} and Yb^{3+} ion concentration levels in the bulk glass sample can be calculated as 3.3×10^{26} ions/m^3 and 6.5×10^{26} ions/m^3 respectively. These doping levels are very close to the specified levels.

Composition	% Weight
Na_2O	8.17
Yb_2O_3	7.77
P_2O_5	69.67
Er_2O_3	3.75
Al_2O_3	11.32

Table 0.1 Composition of the bulk glass sample, obtained using EMP analysis.

3.2.2 Spectroscopy

Any optically amplifying medium must have suitable absorption bands to be pumped with available lasers. In order to identify the various absorption bands and the peak absorption wavelength in each pump band for the Er^{3+} and Yb^{3+} ions in the glass, a transmission spectrum was obtained using a photo-spectrometer. Figure 3.1 shows the % transmission obtained through a polished sample 2 mm thick over a wavelength range from 400 nm to 1600 nm in 1nm intervals.
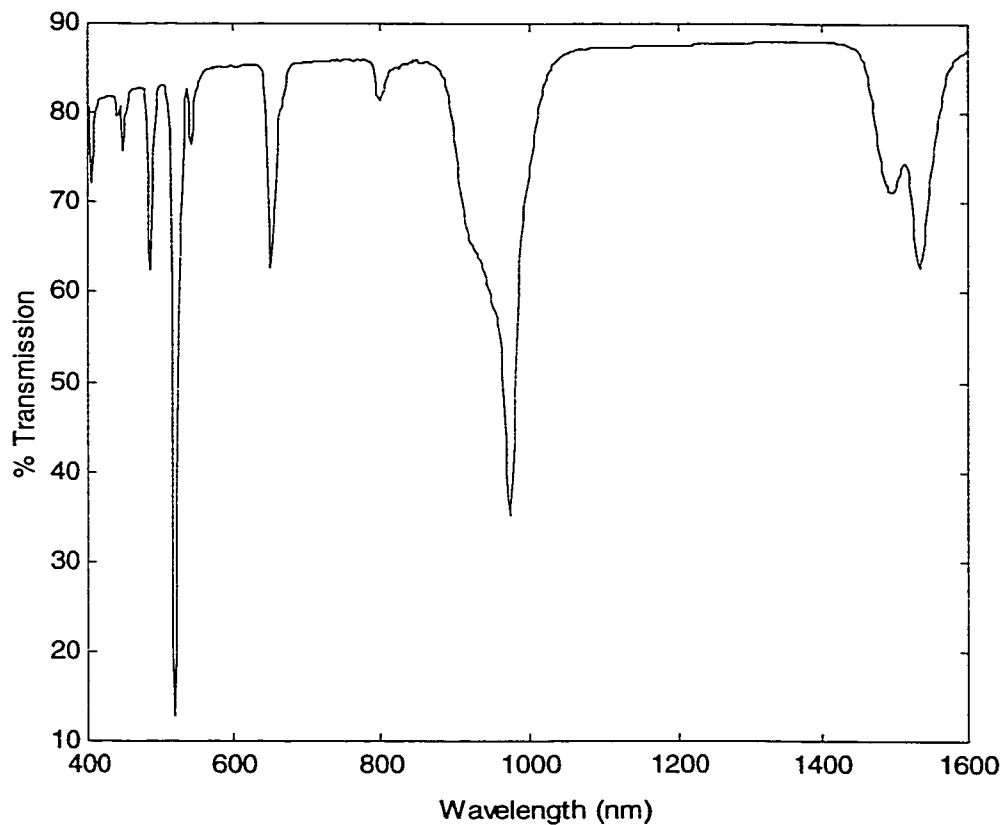
Figure 0.1 Transmission spectrum of the IOG-1 bulk glass.

The peak absorption wavelength corresponding to the $^4I_{13/2}$ manifold of Er^{3+} is identified as 1534 nm. In the shared wavelength region around 980 nm for the $^4I_{11/2}$ manifold of Er^{3+} and the $^2F_{5/2}$ manifold of Yb^{3+} (the only absorption band), the peak is centered at 974 nm. This peak could be identified as corresponding to the $^2F_{7/2} \rightarrow {}^2F_{5/2}$ transition of Yb^+ ions since the absorption cross-section of Yb^+ is an order of magnitude more than

40

that of Er^+ ions at this wavelength (from absorption cross-section data for the IOG-1 glass series [37]). The other absorption peaks for Er^{3+} ions in the near infrared and visible regions are at 800 nm, 651 nm, and 520 nm.

From the transmission data shown in Figure 3.1, the bulk absorption coefficient, α_λ can be calculated as

$$\alpha_\lambda \approx -\frac{\ln(T)}{x} \quad [cm^{-1}] \tag{3.1}$$

$$\approx -\frac{10 \log(e) \ln(T)}{x} \quad [dB/cm] \tag{3.2}$$

where T, is the % transmission and x, is the thickness of the sample in cm. The calculated values are plotted as a solid line in Figure 3.2. At the peak absorption wavelengths of 976 nm and 1534 nm, the bulk absorptions are approximately 22.5 and 10.0 dB/cm respectively (Figure 3.2). This calculation assumes zero reflection from both surfaces of the sample. Including reflections would shift the curve down approximately by 2 dB.
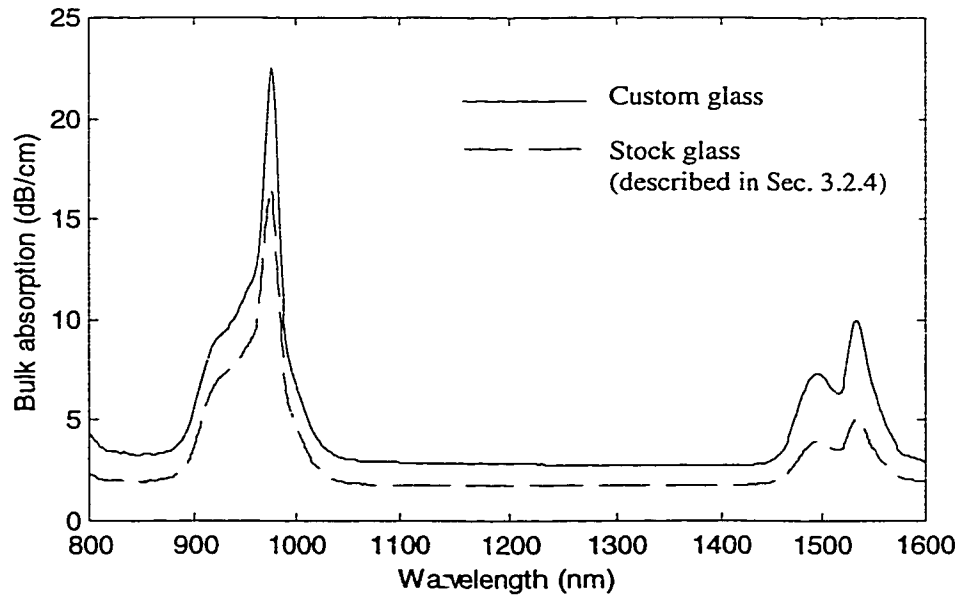
Figure 0.2 Bulk absorption in dB/cm for the IOG-1 custom glass sample (solid line). Dashed line shows the absorption calculated for another glass (stock glass) described in Section 3.2.4.

3.2.3 Photoluminescence properties

As an initial step for characterizing the optical properties of the bulk glass, the photoluminescence (PL) spectra and lifetime were measured for one of the 1mm glass disks described in section 3.2. A connecterised diode laser at a wavelength of 975 nm was used as a pump source to excite the Er^{3+} ions to the $^4I_{11/2}$ mainfold. Using a set of lenses and a chopping wheel, a beam from the fiber patch code was mechanically chopped in free space at a frequency of 10 Hz and a highly collimated beam was shone perpendicularly to the polished surface of the sample. The exiting beam from the other surface was filtered using bare Si wafers to remove any power at the pump wavelength band and detected using a Ge photodetector. The glass was exposed to varying pump power levels up to 100 mW and the florescence decay from the 1540 nm wavelength band corresponding to the $^4I_{13/2} \rightarrow ^4I_{15/2}$ transition was observed using a digital oscilloscope. Decay curves were downloaded to a computer and are plotted in Figure 3.3.
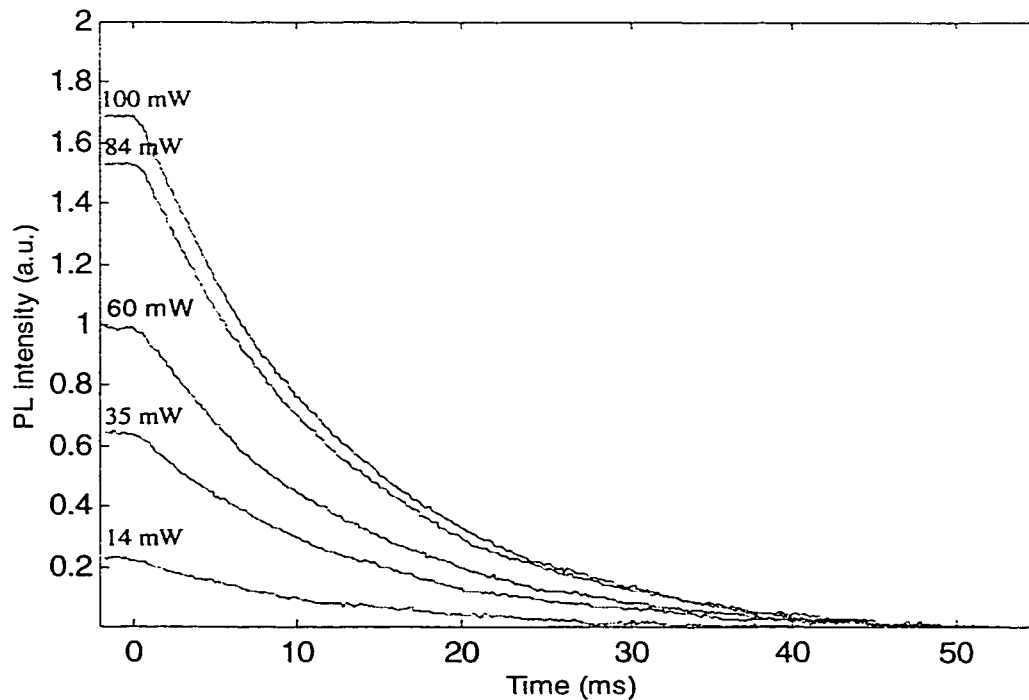
Figure 0.3 Photoluminescence decay curves for the IOG-1 bulk glass sample.

All the curves exhibited a single exponential decay of intensity with time, and the $1/e$ decay time corresponding to the luminescence lifetime was found to be 12.5 ± 0.2 ms. A typical curve in logarithmic format for 100 mW of pump power is shown in Figure 3.4.
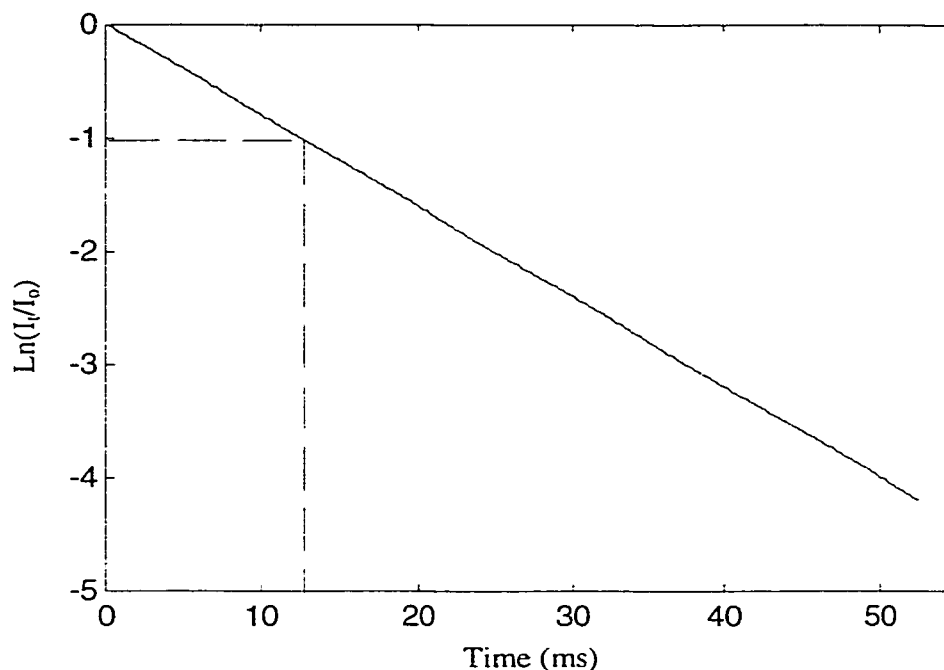
Figure 0.4 PL decay curve in logarithmic format for the bulk glass (for 100 mW of pump power). I_t and I_0 represent the intensity at t ms and 0 ms respectively.

Next, the PL spectrum of the bulk sample in the 1540 nm wavelength band corresponding to the spontaneous emission of Er^{3+} ions from $^4I_{13/2} \rightarrow ^4I_{15/2}$ transition was recorded. For this measurement, the fiber pigtail from the source was directly butt-coupled to the polished surface of the bulk glass sample and the emission was collected using a multimode pick-up fiber. The spontaneous emission signal was analyzed using a monochromator in combination with a Ge PIN detector and the spectral data was downloaded to a computer. Figure 3.5 shows the emission spectra scanned over the wavelength range from 1400 nm to 1700 nm in 1 nm intervals. The peak emission wavelength for the Er^{3+} ions corresponding to $^4I_{13/2} \rightarrow ^4I_{15/2}$ transition occurs at 1534 nm.
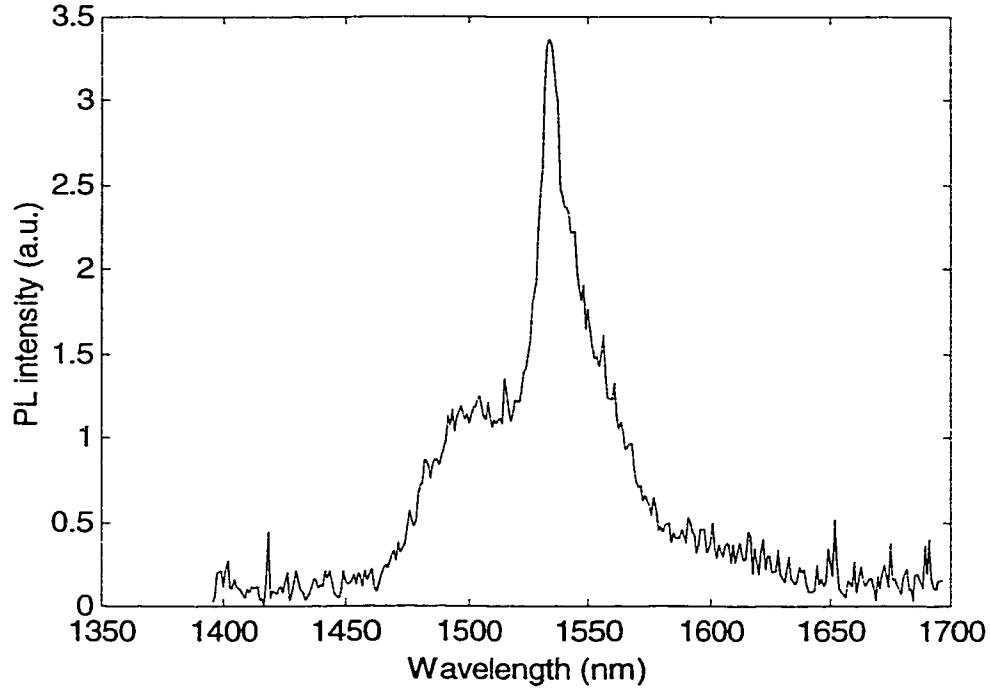
Figure 0.5 Photoluminescence spectra of the IOG-1 Bulk glass sample around 1550 nm wavelength band.

3.2.4 Optical characterization on stock glass samples

Table 0.2 Summary of optical characterization, carried out on stock glass bulk samples.

Rare-earth ions concentration levels *	Er : 1.5×10^{26} ions/m^3
	Yb: 5×10^{26} ions/m^3
Lifetime	11.2 ± 0.2 ms (single exponential)
Peak emission wavelength for Er^{3+} $^4I_{13/2} \rightarrow ^4I_{15/2}$ transition	1534 nm
Bulk absorption peak around 1550 nm	1534 nm (see Figure 3.2)
Bulk absorption at peak	5.1 dB/cm
Bulk Absorption peak around 980 nm	974 nm (see Figure 3.2)
Bulk absorption at peak	16.6 dB/cm

* Specified by the supplier

The same sets of measurements were also carried out on another bulk glass belong to the same IOG-1 phosphate glass series as the custom glass described above. The measured

results are summarized in Table 3.2. These samples, again co-doped with Er/Yb, were purchased from available stock. These stock samples were used in process development while waiting for the shipment of the custom melt samples. The specified refractive index and density of the bulk glass are 1.5196 and 2.75 g/cm^3 respectively. These samples were square with a dimension of 2"×2" and a thickness of 2 mm.

4. Device fabrication

4.1 Introduction

4.1.1 Choice of fabrication processes for waveguide amplifiers

Waveguides in rare-earth doped glass materials have been fabricated by a number of different methods. These include ion exchange, ion implantation, flame hydrolysis deposition (FHD), sol-gel technique, and sputter deposition. In all of these techniques, a composite structure is formed where the light is guided in a high-index core layer, which is surrounded by a low-index cladding layer. The waveguide geometry and the optical properties are generally influenced by the particular technique used for fabrication. Among these, ion exchange and deposition are the two most popular techniques used for making rare-earth-doped waveguide structures.

Since 1972 following the first reported ion-exchanged waveguide by exchange of Tl^+ for Na^+ and K^+ in a silicate glass, much work has been done on various ion pairs and several different glass compositions in developing useful optical waveguides [42]. The advantage of this method is that low-loss waveguides can be made using relatively simple techniques at low cost. In this method, buried slab and channel waveguides are formed by diffusing index-raising materials into the bulk glass. In the case of active waveguides, such as lasers and amplifiers, the rare-earth-doping is realized during the preparation of the bulk glass. In recent years, some good results have been reported with considerable amount of device gain with ion-exchange technique [6]-[8]. However, a drawback in this technique is that only glass substrates can be used for device fabrication.

Ion-implantation is another technique used to prepare Er-doped waveguides. It is a relatively lengthy process where undoped oxide layers (silicate glass [18] and Al_2O_3 films [4]) are first doped with Er ions by MeV ion-implantation and then the appropriate waveguide structures are formed in the Er implanted region.

An Er-doped planar waveguide amplifier [20] and a Nd-doped waveguide laser [21] have also been prepared by FHD using silica-based glasses on silicon substrates. The waveguides show low propagation losses. However, due to low rare-earth doping levels that could be realized in this process, these waveguides are relatively long [20].

The sol-gel method is an attractive technique for integrating rare-earth doped devices with some other optical devices on a single substrate. A multi-component glass mixture is first prepared with the desired portion of rare-earths in the solution and then thin films are deposited on substrates by a dip-coating cycle (substrate is immersed in the solution, withdrawn and dried). Low loss Er-doped Al_2O_3-SiO_2 planar waveguides have been successfully prepared by this sol-gel process with a deposition rate of 36.2 nm per dipping [22].

Radio frequency (rf) sputter deposition, an effective widely used technique to produce dielectric thin film layers, has also been successively used to prepare planar waveguide amplifiers on silicon substrates from Er-doped multi-component silicate [5] and phosphate glasses [11]. A waveguide laser has also been reported using Nd-doped phosphate glass hosts [23]. Unlike the ion exchange process, integration with other optical and optoelectronic devices is possible since Si substrates can be used for device fabrication.

4.1.2 This work

In this study, waveguides are formed by the ion exchange technique. The processes involved in fabricating the waveguide amplifier using the phosphate glasses (characterized in Chapter 3) are described here. Section 4.2 describes the ion-exchange technique in general and the steps taken for fabricating Ag^+-Na^+ ion exchanged waveguides, both slab and channel waveguides, are discussed in Section 4.3. All these processes were carried out using the facilities available at the Micro Fabrication Facility (Micro Fab) of the University of Alberta with the assistance from the Micro Fab staff.

4.2 Ion exchange technique: background

Ion exchange is the simplest method of fabricating low-loss glass waveguides. For a multi-component glass, the refractive index of the glass is related to both the density of the glass and the electronic polarizabilitly of the constituent ions. Glass is usually prepared by melting a number of different mixtures from various oxides such as SiO_2, B_2O_5, GeO_2 and P_2O_5, called network formers, and with a minor portion of network modifiers such as Na_2O, Ca_2O and K_2O. The network modifiers have relatively loose

bonds in the glass network and are added to change the properties of the glass. When glass is heated to higher temperatures the mobility of the cations (positively charged ions from network modifiers) is increased and they are able to move within the glass structure. Other monovalent alkali ions (such as, K^+, Rb^+, Cs^+, Ag^+ and Tl^+) with larger electronic polarizabilitly can then replace the original cations in the glass network through the process of thermal diffusion, referred as an ion-exchange process, where the larger ions diffuse in and replace the out-diffusing original ions from the glass. As a result of the alteration of the electronic structure in the diffused region to that of undiffused regions, the refractive index is locally adjusted and a light guiding buried waveguide structure is formed in the glass. The source to provide the index-raising ions can be in the form of a molten salt bath. The glass substrate is immersed in the salt bath and the ion-exchange process is carried out inside a furnace at an elevated temperature.

Much work has been done on fabricating ion-exchanged waveguides using salt baths to replace various ions in the glass, e.g. KNO_3, $TlNO_3$ or $AgNO_3$ to replace with Na^+, $CsNO_3$ +$CsCl$ to replace with K^+ [43]. When molten salts are used, the exchange of ions occurs only by pure thermal diffusion and the process takes several hours to diffuse the ions deeply under the surface to make single and multimode channel waveguides. However, this process can be accelerated by applying an electric field across the glass sample with the aid of immersed metal electrodes in the salt bath [44],[45]. The applied electric field assists in driving these ions more rapidly towards the negative electrode and causes the ions to be drifted deeply in to the glass.

Recently, waveguide amplifiers and lasers have been fabricated by K^+- Na^+ exchange, using KNO_3 salt baths in multi-component phosphate glasses [6],[7],[24]. Since this is not a dry process, the moisture usually present in the molten KNO_3 salt damages the substrate surface and special care has to be taken to remove the moisture in the salt and to do the diffusion process under vacuum conditions [24].

An alternative approach to make diffused waveguides is to use solid metal thin films on surface of the glass as the ion source. A metal film is directly deposited on the surface of the glass and the diffusion is carried out at an elevated temperature with an electric field applied across the substrate. Among the various alkali ion sources, this

technique is by far mostly used for Ag ion exchange since silver films can be easily deposited and maintained in a stable form [43]. The basic difference in the physics of this process compared to the use of molten salts is that the metal film does not contain the ions but the ions can be released by an electrochemical reaction in which the metal is oxidized (Ag $\rightarrow$ Ag$^+$ + e$^-$) [46]. It should be noted that in the absence of an applied voltage, the ion-exchange is negligible, because the Ag$^+$ atoms can't be ionized in sufficient numbers. Those which are ionized due to the thermal energy distribution can't diffuse into the glass due to the electrochemical potential which is built up between the glass and the silver film [43].

Two advantages of using metal film sources over the salt baths are: (1) the amount of Ag ions diffused into the glass can be easily controlled by the thickness of the film; (2) since the change in refractive index varies directly with the Ag ion concentration in the sample, the index profile can be controlled over a wide range by both the electric field applied and the diffusion time.

4.3 Fabrication of Ag film-diffused ion exchanged waveguides

In this work the diffusion processes or the impact of process parameters on the device parameters are not studied in detail. Rather, after a literature survey on fabrication of single mode (SM) Ag$^+$ film-diffused ion-exchange waveguides [9],[47]-[50] attempts were taken to fabricate SM channel waveguides on IOG-1 bulk glass samples. Ag$^+$ ions were exchanged with Na$^+$ ions in the bulk glass which had a concentration level of around 8-weight % of Na$_2$O$_3$.

4.3.1 Bulk Ag$^+$- Na$^+$ ion exchange in IOG-1 phosphate glass

Initially, the Ag$^+$-Na$^+$ diffusion was tested by preparing some slab waveguides, using the stock glass samples, in order to understand the general behavior of the diffusion process such as diffusion duration and depth for a given set of process parameters. The diffusion depth would give an idea as to how many modes the slab could support in the vertical direction. A polished bulk glass sample 2mm thick was sliced into pieces with a dimension of 1 cm by 2.5 cm. The samples were then cleaned in a pirahna solution (3

parts H_2SO_4 + 1 part H_2O_2) by immersing in the solution for 20 minutes followed by rinsing in de-ionized water and were then blown off using dry Nitrogen.

On one side of the glass pieces, a 0.2 μm thick Ag film was sputter deposited from a 99.99 % pure Ag target to act as the anode and to supply the ions for the diffusion. A deposition system with planar magnetron sputtering gun sources, rotating substrate holder, DC power supply and Ar process gas was used for the metal deposition. On the other side, a 2 μm thick Ag film was deposited to act as the cathode for electrical contact and to sink the out-diffused Na^+ ions from the glass. The diffusion process was carried out using the experimental set up shown in Figure 4.1.
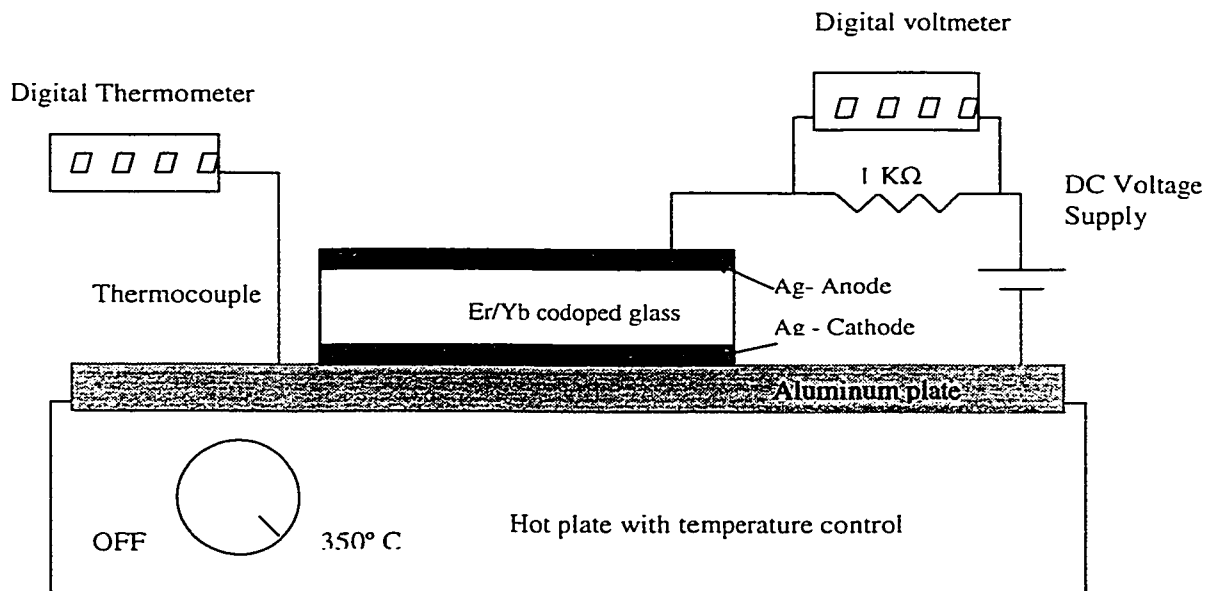
Figure 4.1 Experimental setup for the Ag film diffused ion-exchange in IOG-1 bulk glass.

A hot plate with a temperature control (maximum temperature 350 °C) combined with a thermocouple and a digital thermometer was used to set the temperature for the diffusion process. The sample was placed on the aluminum plate and the temperature was set to 320 °C. The aluminum plate, which was grounded to earth and attached to the ceramic surface of the hot plate, was used to make electrical contact with the cathode side of the sample. A metal-tipped probe was used to make the electrical contact to the anode. A 1 kΩ resister, placed in series with the DC power supply and a digital voltmeter connected across the resister were used to monitor the diffusion current flow through the

glass sample. When the temperature reached a steady value of 320°C, an electrical contact was made to the sample with an applied DC voltage to the circuit. The voltmeter reading was recorded throughout the diffusion duration and when the current flow ceased the sample was disconnected and removed from the hot plate. Figure 4.2 shows the current flow recorded for the applied electric filed of 4 and 6 V/mm across two samples.
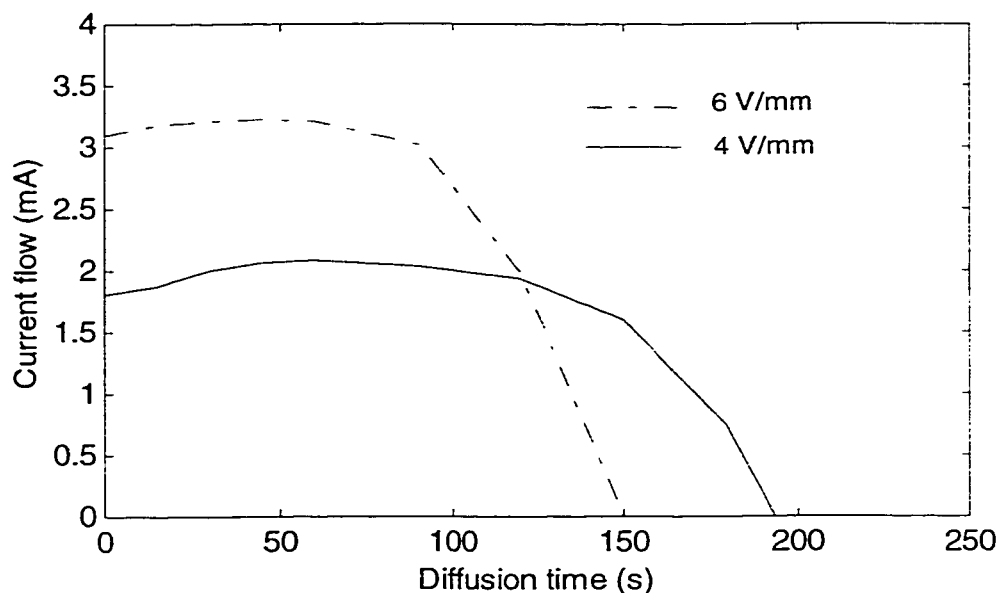
Figure 4.2 Diffusion current flow through a 2mm thick IOG-1 bulk glass sample for applied electric fields of 4 and 6 V/mm at 320°C.

For both samples current flow reached a steady state value immediately after the voltage was applied. This indicates that the sample had reached the thermal equilibrium and mobility of Ag ions achieved a steady value. As more and more Ag ions diffused into the glass, depletion of the Ag source at the anode caused the current flow to begin to drop after some time and ceased when the Ag source was fully depleted.

For a given thickness of Ag film, the magnitude and the shape of diffusion current varies with the applied electric field. The maximum diffusion current increases with increasing electric field. The higher the voltage, the larger the number of ions capable of overcoming the electrochemical barrier potential at the interface. The process duration decreases with increasing diffusion current. This is expected since the total amount of silver ions diffused into the glass in both cases is constant and is a function of total

current flow through the sample. This can be shown by integrating the diffusion current (*i*) verses time (*t*) curves in Figure 4.2, resulting in the same total charge, Q ($Q = \int i \, dt$).

After the diffusion process, the samples were cleaned by immersing in metal etchant to remove the silver residue on the glass surfaces. Then the samples were cut and the edges were fine-polished. The samples were examined by placing them in a SEM and the back- scattered electrons were used to image the diffusion profile across the polished edge of the samples. Figure 4.3 shows the image taken from a sample, ion-exchanged with 6 V/mm of electric field. As can be seen, the regions where silver ions diffused look brighter than the substrate. The depth down to negligible diffusion is approximately 5.5 μm. This value is very close to the diffusion depth obtained in fabricating single mode waveguides in Er/Yb doped silicate glass with the same set of process parameters [9].
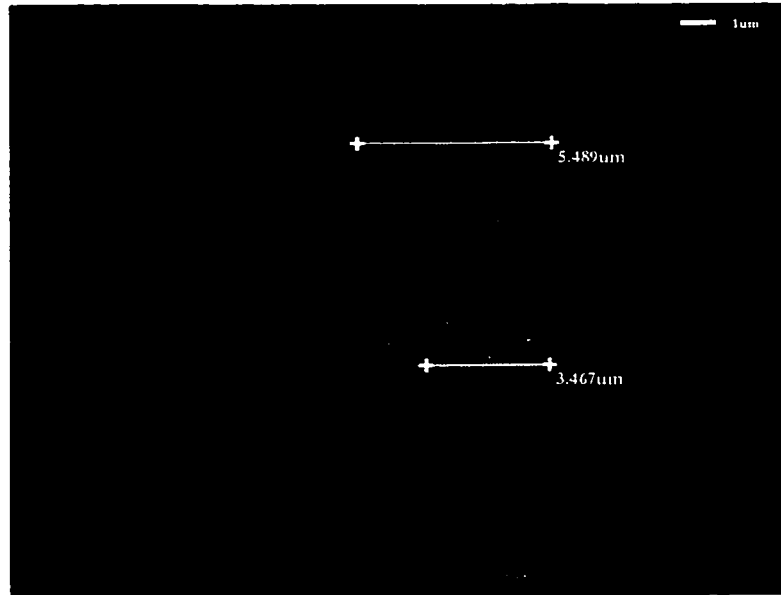
Figure 4.3 SEM photograph of the Ag film ion-exchanged slab waveguide with an applied electric field of 6 V/mm, at 320°C.

4.3.2 Fabrication of silver film diffused channel waveguides

To make two-dimensional waveguides, the diffusion of the silver ions need to be restricted in a direction perpendicular to the direction of propagation along the waveguide. A thin film layer with narrow openings, placed between the surface of the

sample and the silver film ion source would permit in making two-dimensional channel waveguides, allowing silver ions to diffuse only through the narrow openings. A photo-mask with a wide range of openings, from 5 to 10 μm, was designed and developed with a view to making single mode channel waveguides at both signal (1550 nm) and pump (980 nm) wavelengths, allowing for any tolerances in the process parameters.

1. Chrome deposition (masking layer)

2. Spinning Photo-Resist followed by soft bake and UV exposure

3. Developing the photoresist

4. Chrome etch and then stripping off photoresist
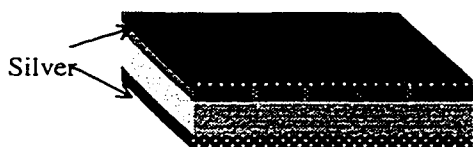
5. Deposition of silver on top and bottom
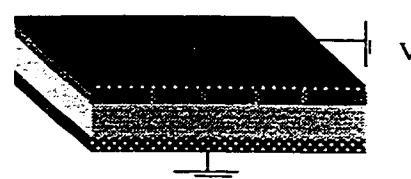
5. Electric-field-assisted Ag^+-Na^+ exchange at an elevated temperature

Figure 4.4 Steps followed in fabricating channel waveguides in IOG-1 bulk glass.

The process steps involved in fabricating channel waveguides are shown in Figure 4.4. The process was first performed on a 2"x2"x2 mm stock glass sample. Initially, as the masking layer, a 0.2-μm thick chrome layer was sputter-deposited on the surface of the pre-cleaned sample by DC sputter deposition. Then by photolithography and wet

etching (see Appendix A for the details) the waveguide patterns in the photo-mask was transferred to the chrome layer (steps 2 through 4 in Figure 4.4). As we see in step 4, the chrome layer has been selectively removed to form openings that are needed for silver diffusion.

Silver layers 0.2 μm and 2 μm thick were then sputter-deposited on top of the patterned chrome layer and on the other side of the sample respectively. Silver diffusion was carried out with an applied electric field of 4.5 V/mm at 325 °C. A maximum current flow of 9.6 mA was noted and the process was stopped after 10 minutes when the current flow dropped to a negligible value (< 0.5 mA). Finally, all the remaining metal layers in the sample were removed using metal etchants and the sample was cleaned and dried.
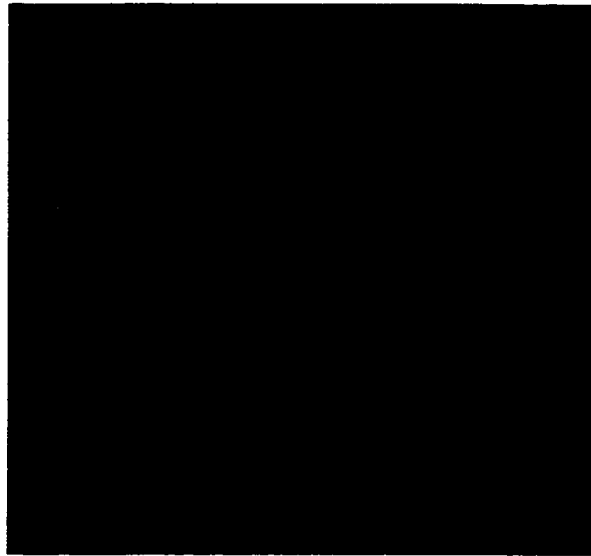
Figure 4.5 SEM photograph of silver-film diffused channel waveguides on stock glass.

Figure 4.5 shows a SEM photograph of the channel waveguides fabricated using the above process. The spacing between the waveguides is 200 μm. The width of silver diffused area is around 20 μm, which is much wider than the corresponding openings of ~ 7 μm in the patterned chrome layer. This lateral diffusion under the masking region in the proximity of openings has been reported in fabricating channel waveguides using electric-field-assisted silver film ion exchange [9],[46],[48]. Some authors have paid attention to this problem, analyzing this effect observed under various set ups for the

54

diffusion processes such as different masking layers both conductive and insulating, and with and without any external applied electric field. However, the explanations given contradict each other and no clear conclusion has yet been drawn to understand the mechanism for the side diffusion under the mask openings [43],[51].

Channel waveguides were then formed on the custom glass by following the same process steps as described above. The thickness of the glass sample was 1mm. The thickness of the metal layers and the process parameters for Ag^+-Na^+ ion-exchange process were kept unchanged in a view of reproducing similar waveguides as in the stock glass.
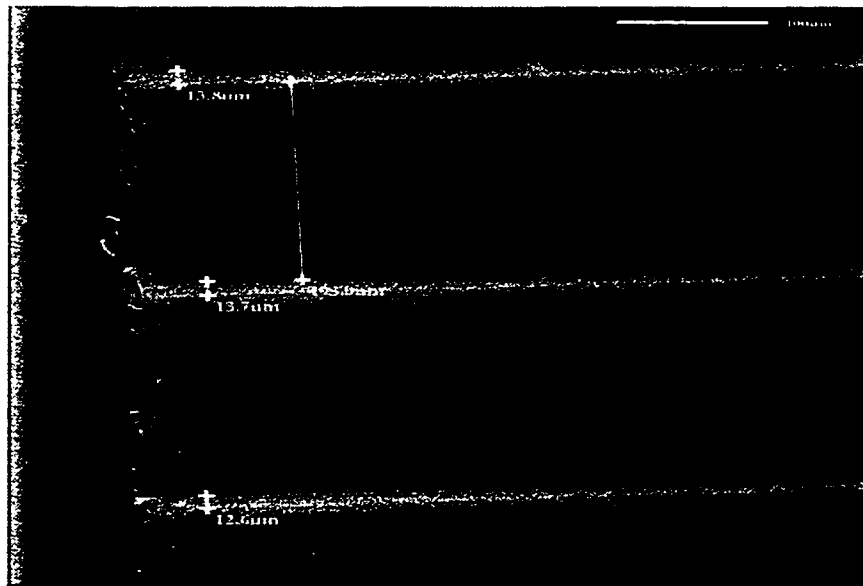
Figure 4.6 SEM photograph of Ag-Na ion-exchanged waveguides fabricated on 1 mm thick custom sample.

Figure 4.6 shows the SEM photograph of some of the Ag^+-Na^+ ion-exchanged waveguides fabricated on the 1 mm-thick custom sample. The width of the diffusion area on this sample was found to be 13-15 μm.

5. Optical characteristics and gain performance of Ag-Na ion-exchanged channel waveguides

This chapter presents the experimental work carried out on the ion-exchanged waveguides, fabricated in two different IOG-1 bulk glass samples, as described in Chapter 4. The experimental set-up for optical characterization and gain performance, and the results obtained, are given and discussed. The diffused samples were saw-cut into different waveguide lengths and the waveguide ends were mechanically polished to obtain optimal light coupling to the waveguides.

5.1 Optical characterization of diffused waveguides in stock glass samples

The photoluminescence lifetime corresponding to the $^4I_{13/2} \rightarrow ^4I_{15/2}$ transition of Er^{3+} ions was measured using a 976-nm wavelength diode laser pump source. The experimental set up for this measurement is shown in Figure 5.1. The light from the pigtailed laser was first passed through a fiber collimator (an assembly of a collimating lens and a fiber connector) and a collimated beam in free space was produced. The beam was then focused using a lens and chopped at the focal point using a mechanical chopper at a frequency of 15 Hz. The chopped beam was again collimated and coupled back to a single mode fiber by repeating the arrangement of a lens and a fiber collimator. The fiber was then butt-coupled to the waveguide. The alignment of the fiber to the waveguide was obtained by mounting the fiber on a three-axis micro-positioner.

The emission from the waveguide output was collected using a multimode pickup fiber. The pump beam was totally filtered out by using two fiber isolators in series. The pass band of the isolators was 1550 ± 30 nm and each offered a loss of 41 dB at 980 nm. A InGaAs high-speed PIN detector with a multimode fiber pigtail assembly was used to detect the signal at the isolator end. The electrical signal was then amplified and observed on a digital oscilloscope. For an input pump power of 32 mW, the decay data obtained is plotted as a solid line in Figure 5.2. The data obtained from the bulk glass (single exponential decay, as discussed in Sections 3.2.4) is also shown in Figure 5.2 (broken line). As can be seen, the measured decay deviates from a single exponential and has a fast initial decay, indicating that the Er^{3+} ions are being removed from the metastable

state ($^4I_{13/2}$) by ion-ion interactions, such as pair-induced or co-operative upconversion effects. Further, bright green luminescence observed along the waveguide is evidence of upconversion or excited state absorption occurring in the $^4I_{11/2}$ energy level for Er^{3+} ions (Sections 2.3.2. and 2.3.3.). From this measured data, the $1/e$ lifetime was estimated as 4 ± 0.5 ms.
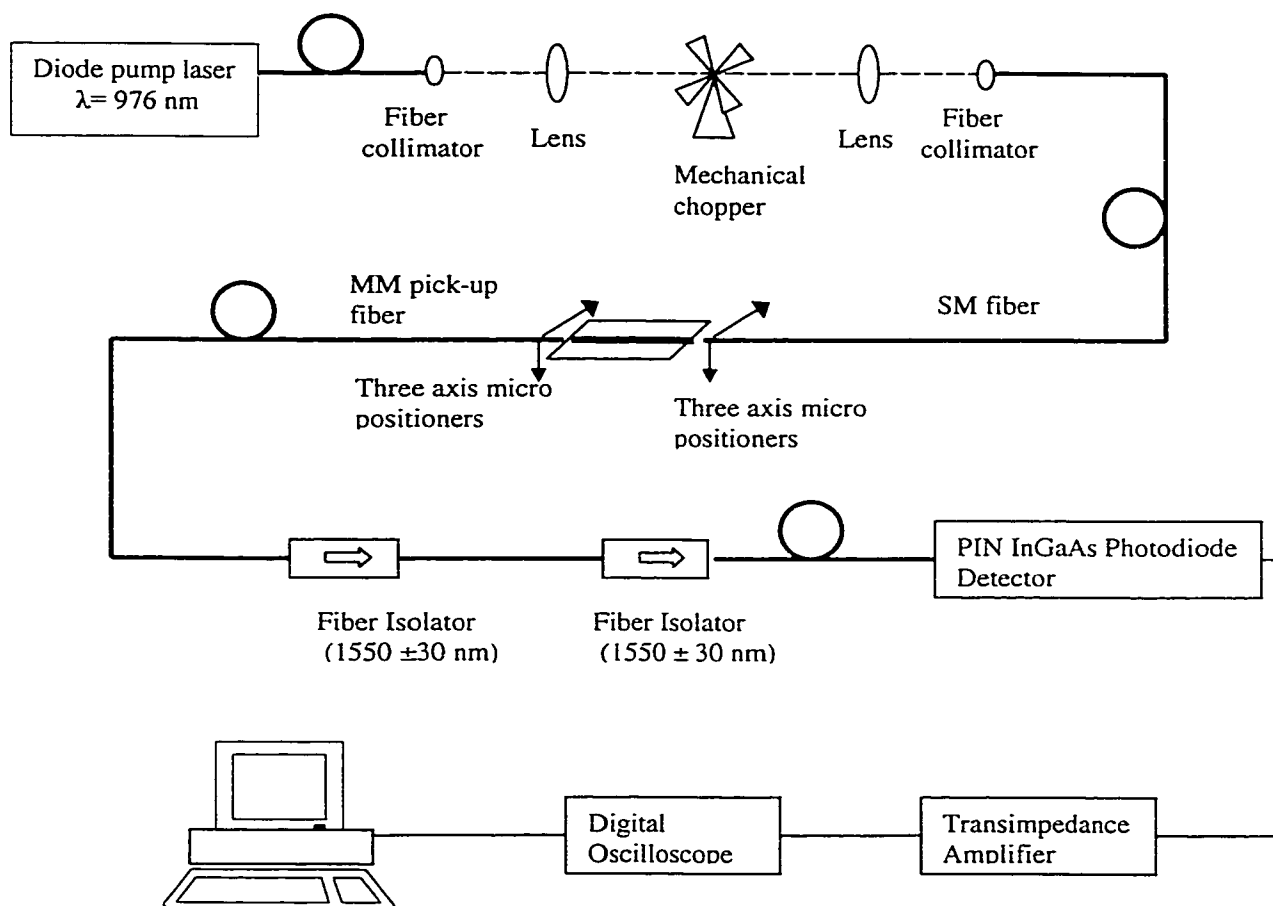
Figure 5.1 Set up for the photoluminescence lifetime measurements in ion-exchanged waveguides.
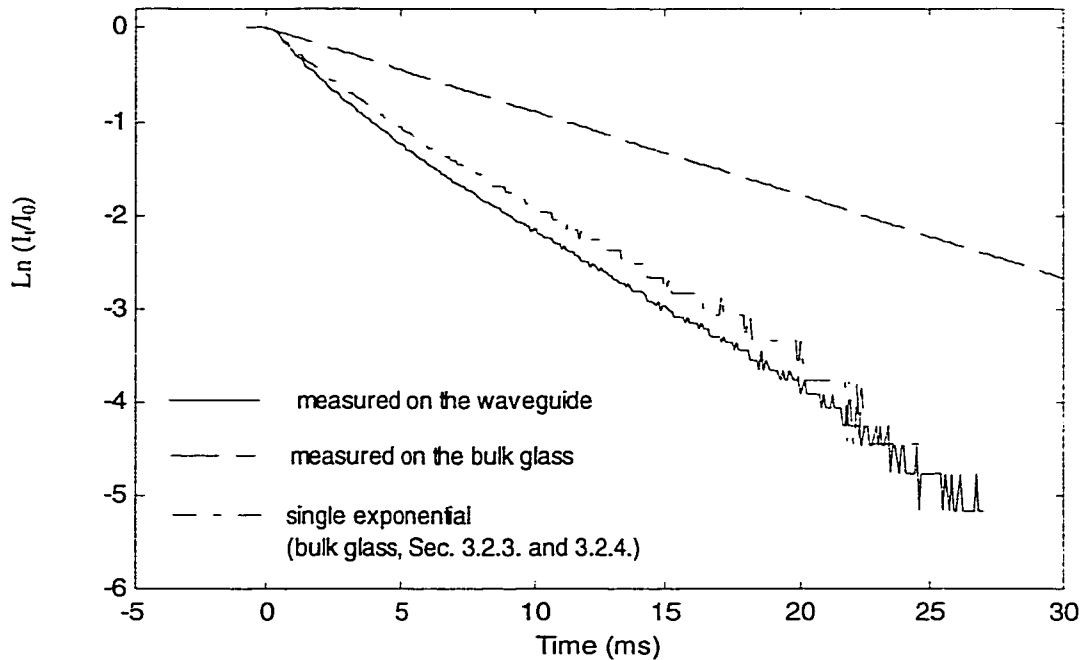
Figure 5.2 Photoluminescence intensity decay in ion-exchanged waveguides formed on stock glass samples (solid line) and compared with data obtained in the bulk glass: free-space coupling (broken line), fiber butt-coupling (dash and dot line). I_t and I_0 represent the intensity at t ms and 0 ms respectively.

Upconversion processes are the main gain-limiting mechanisms in heavily Er-doped waveguides and at high pump intensities [16],[18]. It should be noted that the pump intensity is at least six orders of magnitude higher in the case of fiber-waveguide coupling than in free space surface coupling via a 3 mm spot collimated beam (Sec. 3.2.3). In order to measure the lifetime of the bulk glass at high pump intensities, the input fiber was butt-coupled to the polished surface of a 2 mm thick bulk glass sample, and the emission through the sample was measured and recorded. This data is also plotted as a dash and dot line in Figure 5.2. The 1/e lifetime, for this decay, was estimated as 4.5 ± 0.5 ms. The fact that this lifetime remains close to the value that is obtained from the waveguide clearly shows that the huge reduction in lifetime is due to the upconversion process, activated at high pump intensities. Also, the silver diffusion process did not significantly alter the lifetime for Er^{3+} ions in the glass.

Next, the Er^{3+} luminescence spectrum at the 1550 nm wavelength band was measured using the set-up shown in Figure 5.3. Again, the pump beam at 976 nm was used to excite the Er^{3+} and Yb^{3+} ions in the absence of any signal around 1550 nm

coupled to the waveguide input. The signal at the output was collected with a 62.5 μm multimode fiber and analyzed using a monochromator (Digikrom 240) in combination with a Ge PIN diode. The data from both the monochromator and the power meter were downloaded to the computer. For a coupled pump power of 80 mW into a 1.5 cm waveguide, the normalized luminescence intensity obtained in 0.1 nm intervals was plotted as shown in Figure 5.4 (solid line). The emission peak is at 1534.6 nm and the FWHM is 29 nm (from 1525.6 nm to 1554.6 nm). Comparison with the bulk emission spectra (broken line) shows the emission peak and the spectral shape are preserved after the Ag diffusion process.
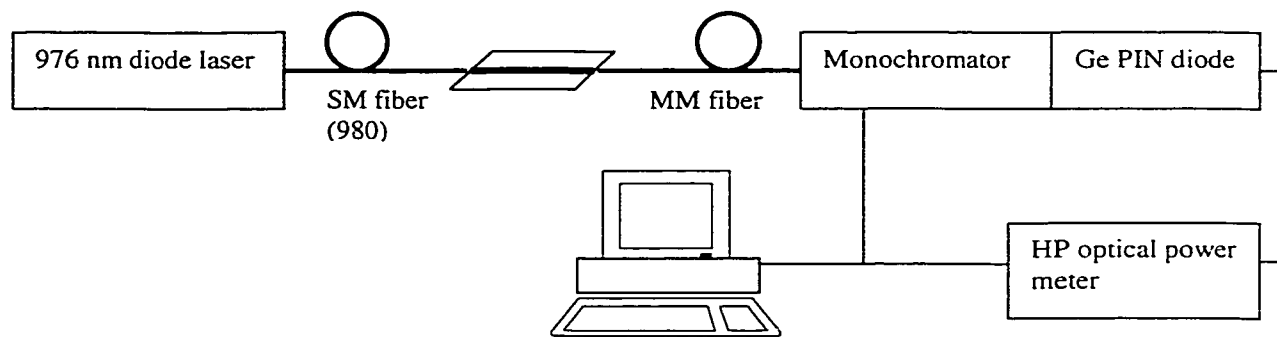
Figure 5.3 Experimental set up to measure the luminescence spectra in diffused waveguides.
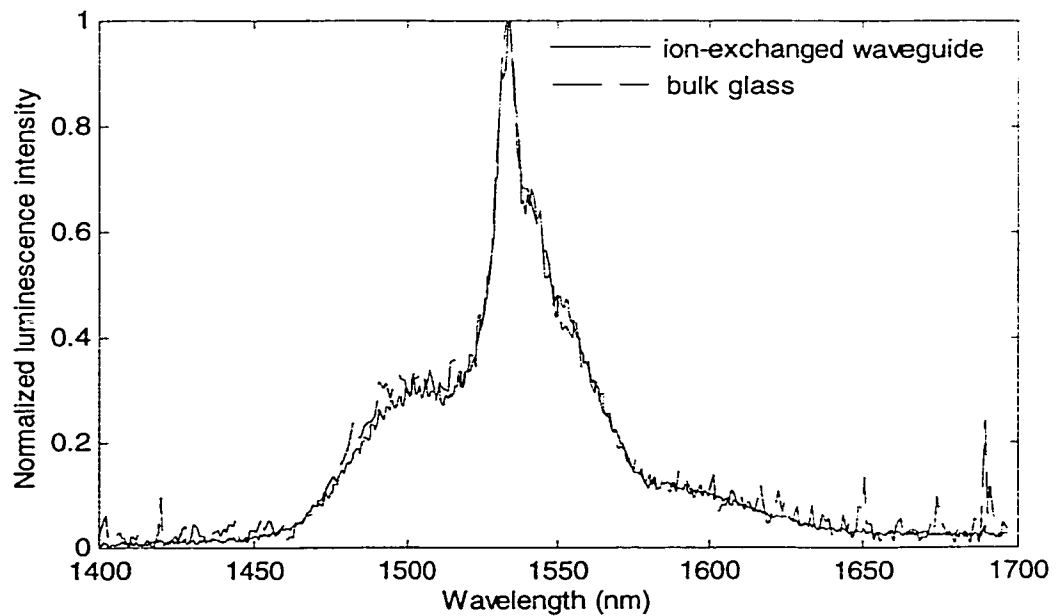
Figure 5.4 Photoluminescence spectra in Ag-film ion-exchanged waveguides compared with the spectra obtained in the bulk glass.

5.2 Optical amplification measurements on stock glass samples

Optical gain measurements were carried out on the ion-exchanged waveguides using the setup shown in Figure 5.5. The signal from a 1533.5 nm laser diode was coupled with the pump at 976 nm using a WDM and the combined signal was butt-coupled to the waveguide input. The wavelength spectra of signal and pump used in this measurement are shown in Figure 5.6. The signal power was kept at 80 μW at end of the input fiber. The signal at the output of the waveguide was collected with a multimode pickup fiber (62.5 core diameter) and passed to a Ge detector through an assembly of silicon wafers to filter out all pump light. An index-matching fluid was used at both ends of the waveguide to reduce the fiber-waveguide coupling losses. The waveguide tested was 1.5 cm . Initially, the ASE around 1550 nm was measured at different pump powers without any signal fed to the waveguide to calibrate the detector assembly. At zero pump power, the total measured signal loss (fiber-to-fiber) in the waveguide was 7.8 dB. This loss is the addition of the absorption by Er ions, waveguide scattering loss (or background loss) and the coupling loss. The total loss measured at a wavelength of 1320 nm (non-absorption wavelength for both Er^{3+} and Yb^{3+} ions) was 1.01 dB. The enhancement of the signal intensity measured at the pickup fiber as function of pump power at the input fiber is shown in Figure 5.7. The error margin in each measurement based on repetitive measurements amounted to ± 0.2 dB.
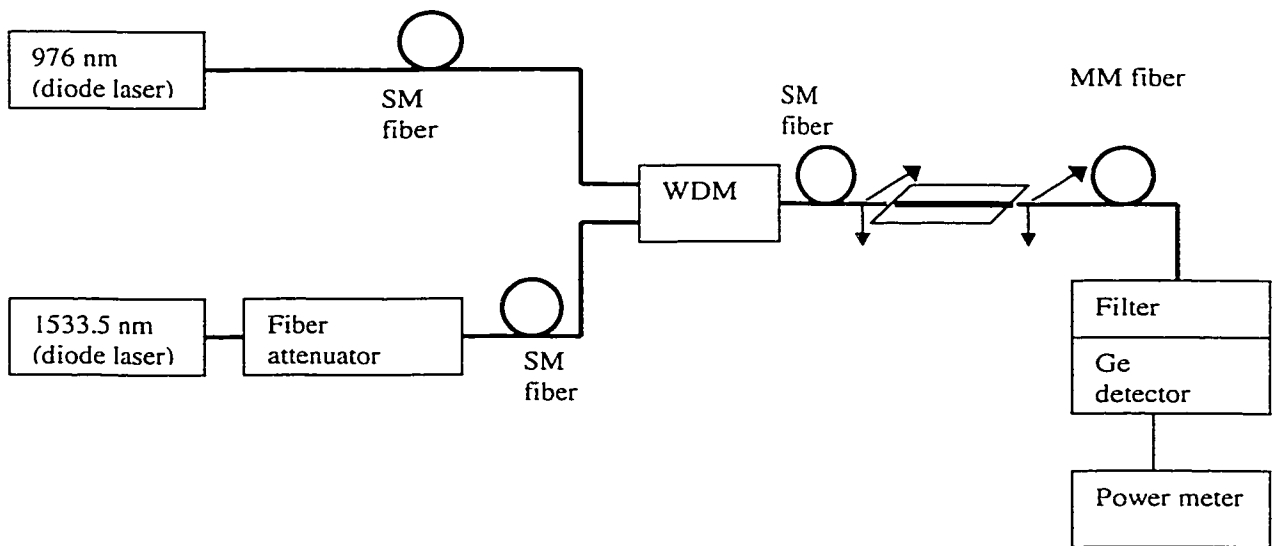
Figure 5.5 Experimental setup for gain measurements in the ion-exchanged waveguides.
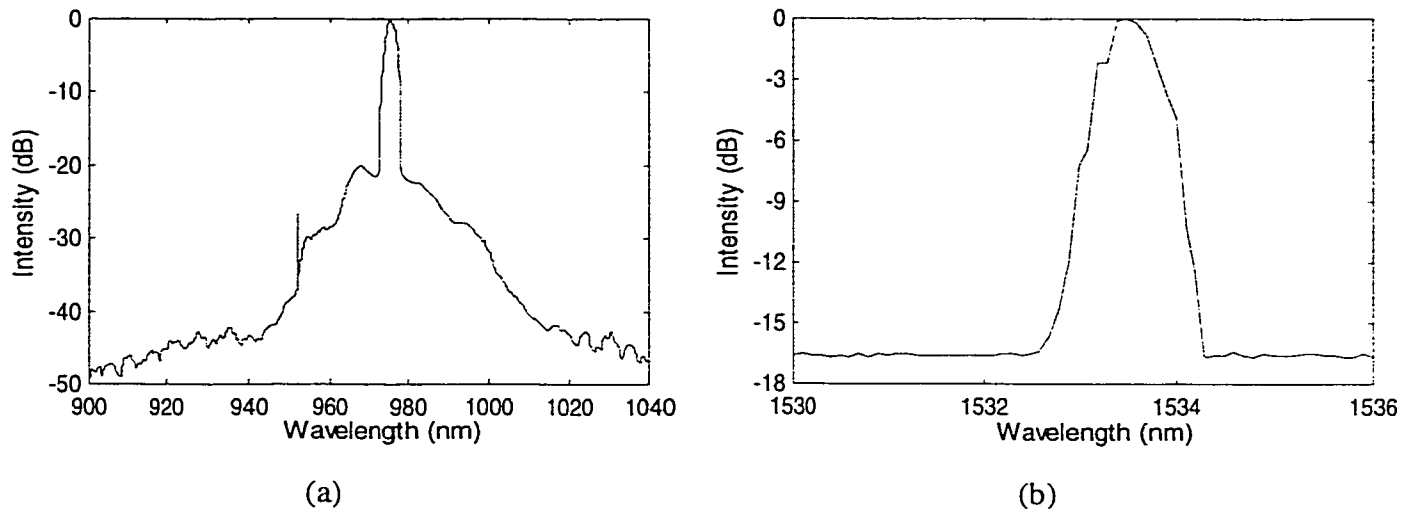
Figure 5.6 Spectra of signal (a) and pump (b) used in the gain measurements. Peak wavelengths for signal and pump are 1533.5 nm and 976 nm respectively.
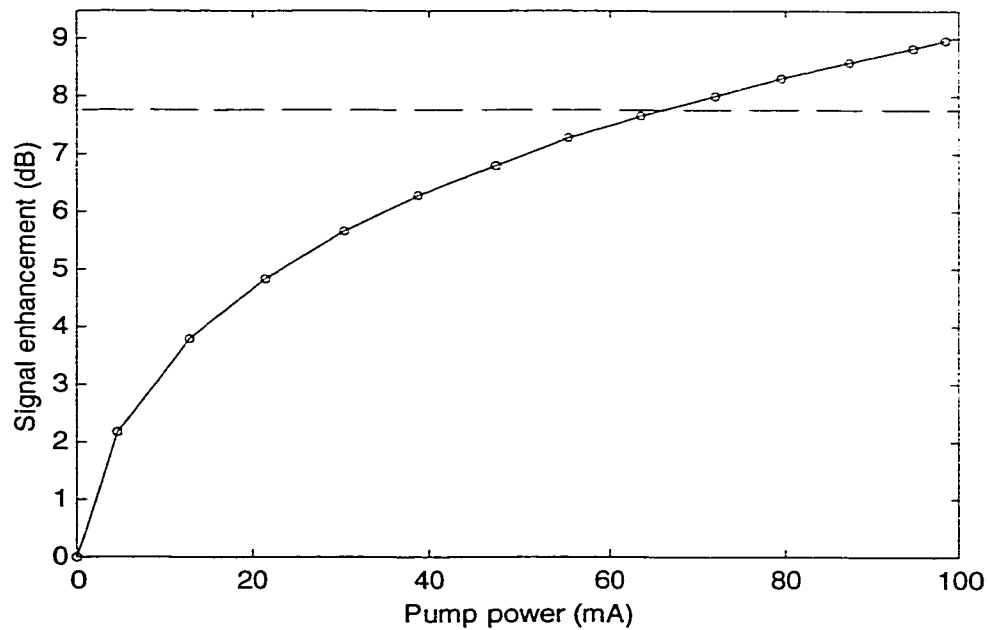
Figure 5.7 Measurements of transmitted signal enhancement at 1533.5 nm as function of pump power (at the input fiber end) in a 1.5 cm Ag-Na ion-exchanged waveguide. Input signal power was 80 μW (-11 dBm). Dashed line shows the total signal loss at zero pump power.

As seen in Figure 5.7, the signal power increases as pump power is increased and at a power level of 66 mW the total signal loss in the waveguide is recovered. A further

61

increase in pump power produces net gain in the device and 1.2 dB system gain is realized at 98 mW of pump power (limit of the laser). Further, the curve indicates that the optimum gain or the gain saturation for this waveguide was not achieved within the range of pump powers used in the measurements.
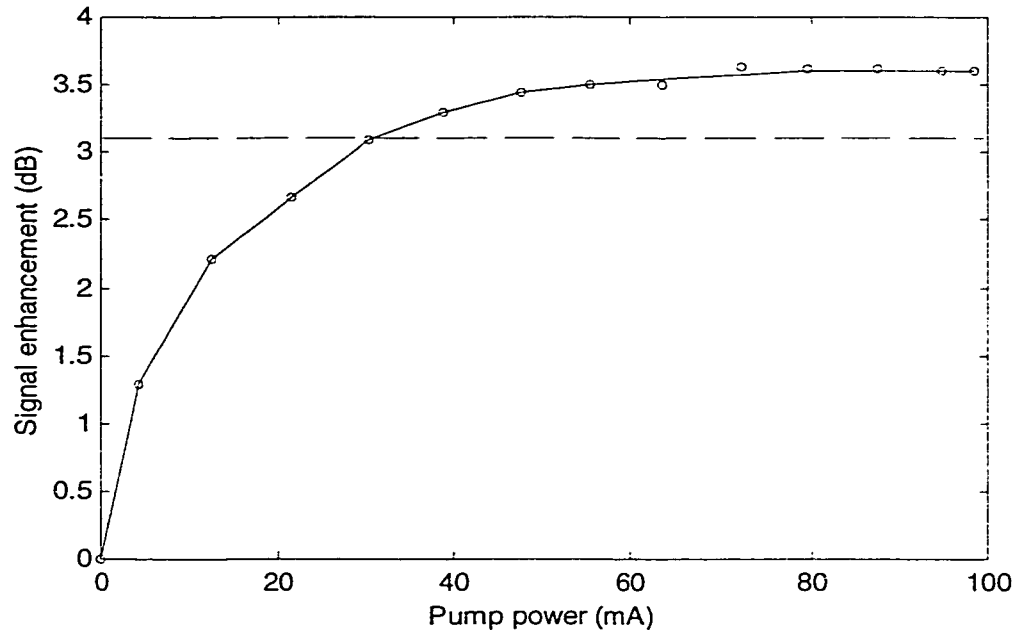
Figure 5.8 Measurements of transmitted signal enhancement at 1533.5 nm as function of pump power (at the input fiber end) in a 0.5 cm Ag ion-exchanged waveguide. Input signal power was 80 μW (-11 dBm). Dashed line shows the total signal loss at zero pump power.

With a view to measuring the gain coefficient (gain per cm) for this waveguide, a shorter waveguide, 0.5 cm in length, was obtained by sawing the 1.5 cm waveguide. Figure 5.8 shows the enhancement in signal intensity as a function of pump power. The total signal loss in this waveguide was 3.12 dB. The maximum signal enhancement of 3.61 dB was realized in this shorter waveguide at pump powers as low as ~ 55 mW. The gain saturation achieved at this pump power level indicates that the total population inversion for Er^{3+} ions is realized throughout the length of the waveguide. From the fiber-to-fiber loss measurements obtained at 1320 nm for the waveguide at the two different waveguide lengths, 0.5 cm (0.77 dB) and 1.5 cm (1.01 dB), the background waveguide loss or the scattering loss, was estimated as 0.24 dB/cm. By assuming the scattering loss

at 1533.5 nm, equal to that of 0.24 dB/cm at 1320 nm, and by interpolating the losses measured at 1533.5 nm, the Er absorption loss in the waveguide was estimated to be 4.35 dB/cm. The coupling loss at 1533.5 nm, at both facets, was estimated to be 0.87 dB. The internal gain of the 0.5 cm waveguide can then be calculated as 1.36 dB (3.61 dB-3.12 dB + 0.87 dB), which gives a gain coefficient for the waveguide of 2.72 dB/cm.

The total ASE noise power in the signal band for this 0.5 cm waveguide was measured as 6 μW when the waveguide was pumped at 98 mW of power. Both the signal and the ASE power levels at the output of the waveguide, measured with the monochromator, are plotted in Figure 5.9. The input signal power was 80 μW (-11 dBm). The plot shows the in-band signal-to-noise ratio to be approximately 30 dB. Note that the intensity readings are not calibrated to the monochromator insertion loss since only the relative power levels were sought here.
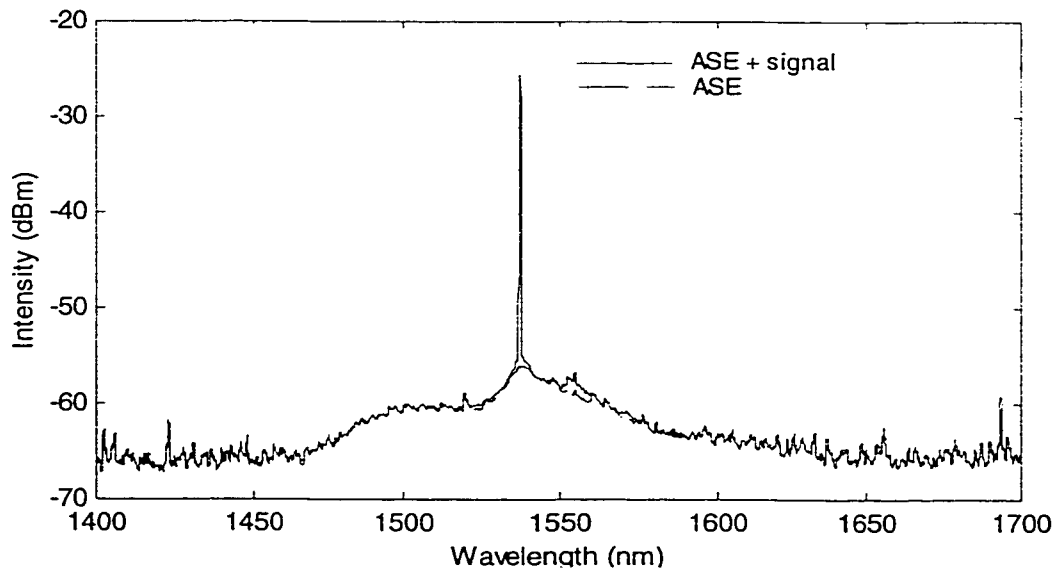
Figure 5.9 The signal and ASE noise levels at the output of the 0.5 cm waveguide. The input power levels for signal and pump are 80 μW and 98 mW respectively.

Figure 5.10 shows the pump absorption measured in the 0.5 cm waveguide as a function input pump power. While gain saturation was achieved at pump power levels above 55 mW (Figure 5.8) the pump transparency (or no further absorption) is not achieved for power levels up to 98 mW (Figure 5.10). This indicates that ground level

Yb^{3+} ions are still available in the waveguide, but the Er^{3+} ions are completely inverted, resulting in gain saturation.
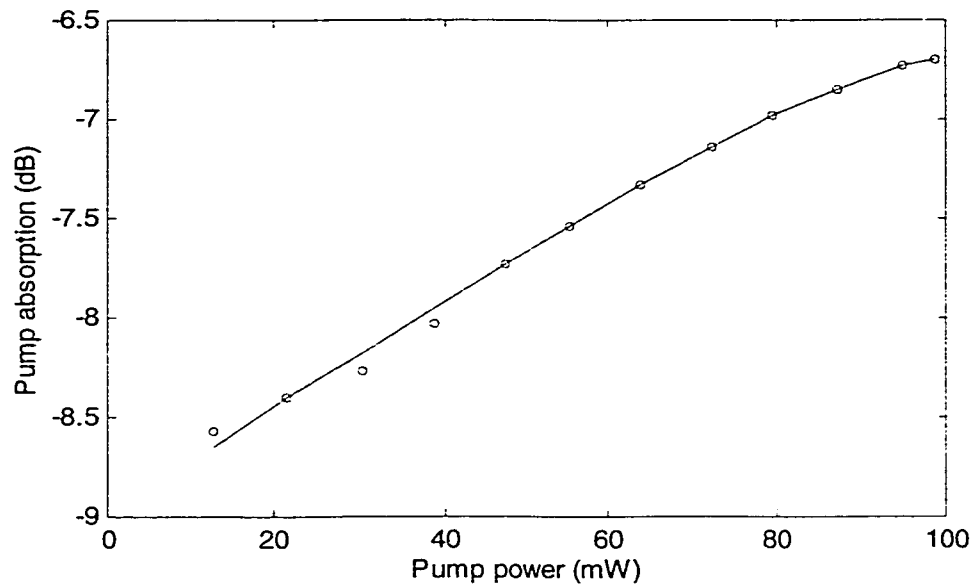
Figure 5.10 Pump absorption versus input pump power in the 0.5 cm Ag ion-exchanged waveguide.
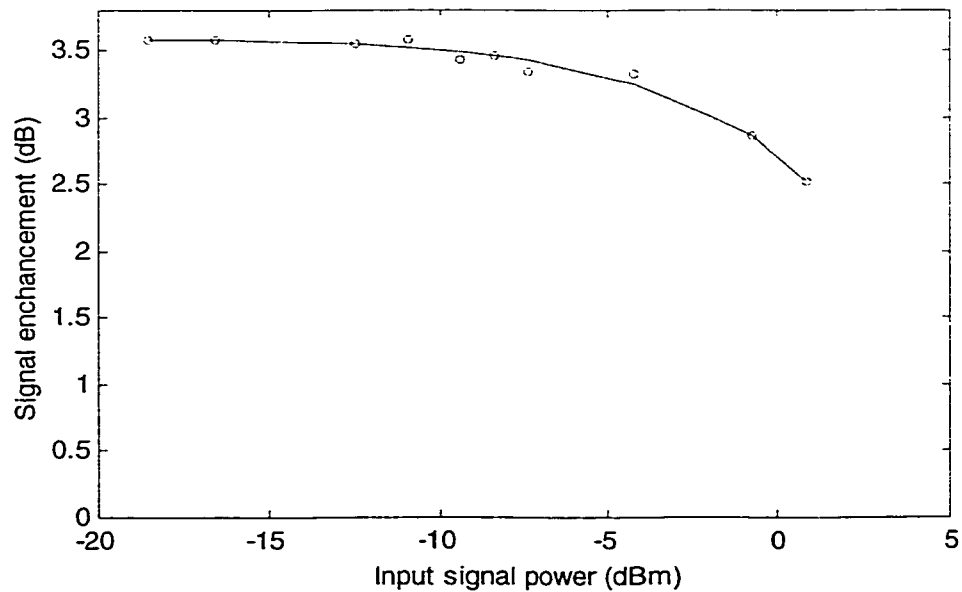
Figure 5.11 Signal enhancement as a function of input signal power in the 0.5 cm waveguide. Input pump power was kept fixed at 70 mW.

Another important amplifier characteristic is the output saturation power. Figure 5.11 shows the signal enhancement as a function of input signal power measured for the 0.5 cm waveguide. The pump power was kept fixed at 70 mW. As seen, in the small-signal regime the signal throughput is independent of the input signal power but when input signal power exceeds −8 dBm the signal enhancement decreases with increasing input signal power. This behavior is as due to signal saturation and it occurs when the signal power approaches to that of the pump power in the waveguide [34]. As signal increases in power past the small signal value, the gain decreases since the pump can no longer replenish the inversion as fast as the signal depletes it. Consequently more pump power is required to realize the same level of signal amplification in the device.

5.3 Optical measurements on Ag-Na ion-exchanged waveguides formed on the custom glass

The optical characteristics of the waveguides formed on the custom melt glass were examined with the setup as described in section 5.1. The photoluminescence decay curves were observed to be multi-exponential and the lifetime measured at 30 mW of pump power was 2.0 ± 0.5 ms. The drop in lifetime (from bulk to waveguide) in this glass is more than that found in stock glass. The reason could be possibly due to the high doping level of Er^{3+} ions (3.2 × 10^{26} ions/m^3, twice that in stock glass) in the custom glass. The measured photoluminescence spectral shape was found to be similar to that obtained from the bulk (custom) glass (Figure 3.5) and peaked at 1534.6 nm.

The optical gain measurements were then carried out using the same setup as described in Section 5.2. The waveguide under test was 0.5 cm. The total throughput signal loss (fiber-to-fiber) in this waveguide was measured as 5.65 dB. Figure 5.12 shows the enhancement in signal power as a function of input pump power. Signal enhancement of 3.68 dB was obtained at 98 mW of pump power. The rate of increase in the signal power with increasing pump was unexpectedly lower than that obtained with waveguides formed in the stock glass (Figures 5.7, and 5.8), though the custom glass had a higher concentration level of Er^{3+} ions. Also, the curve indicates that the predicted maximum (or

the saturated) signal enhancement falls bellow the 5.3 dB level needed to compensate the signal absorption in the waveguide.
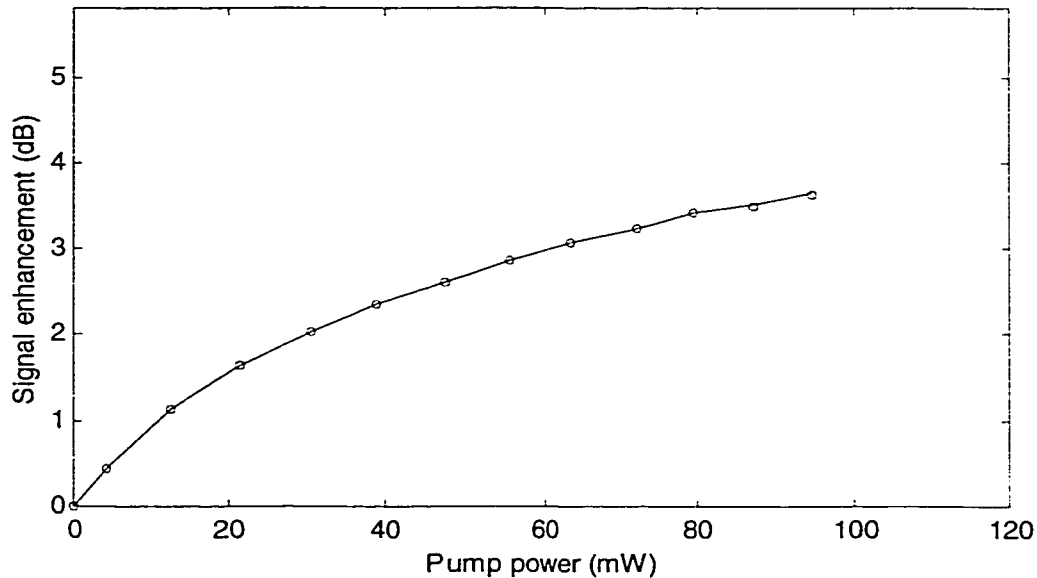
Figure 5.12 Measurements on signal enhancement as function of input pump power in 0.5 cm Ag-Na ion-exchanged waveguide fabricated using custom melt glass. Input signal power was 80 μW.

The throughput loss (fiber-to-fiber) measured at 1320 nm was 1.7 dB. Assuming the coupling loss in this waveguide to be close to that calculated from the waveguide characterized in the previous section (~ 0.9 dB) the waveguide background loss can be estimated as 0.8 dB, i.e., 1.6 dB/cm.

5.4 Discussion

The waveguide formed in the stock glass showed a net gain (1.36 dB) at reasonable pump powers. Relatively low waveguide loss (0.24 dB/cm) realized in the waveguide allowed net gain at an Er^{3+} concentration level of 1.5×10^{26} ions/m^3. The gain measurements performed at different input signal powers (the small-signal regime in Figure 5.11) shows the consistency in realizing net signal gain in the device. The net gain can be further increased in these waveguides using longer devices by pumping at higher power levels. Either a high power pump source or a bi-directional pumping scheme (pumping from both ends of the waveguide) can be used to provide sufficient power throughout the extended length of the waveguide.

As for the waveguide formed in the custom glass, the signal enhancement was insufficient to overcome net signal throughput loss. Higher waveguide loss (1.6 dB/cm) together with the reduction in the lifetime for Er^{3+} ions resulted in poor amplifier characteristics in this waveguide. The excess propagation loss of 1.6 dB/cm was higher than expected (compared to 0.24 dB/cm of waveguide loss in the stock glass). The custom glass appeared to be less transparent than the stock glass after the diffusion process, although similar process parameters were used for the Ag^{3+}-Na^{3+} ion-exchange process in both glasses. Also, the bulk absorption determined using the photo-spectrometer (see Figure 3.2) indicates that the custom glass had more absorption (approximately by 1 dB/cm) than the stock class at wavelengths around 1320 nm (non-absorption wavelengths for Er^{3+} and Yb^{3+} ions). Moreover, the slope of the curve as shown in Figure 5.12 indicates that the pump energy is not efficiently converted in improving the signal intensity. This behavior could have resulted from the non-homogeneous distribution or the clustering of the active ions in the glass. The clustering effect not only increases the upconversion, both co-operative and pair-induced upconversion, but also minimizes the possibility of any energy transfer between neighboring Er^{3+} and Yb^{3+} ions.

Figure 5.13 Photograph showing the green light emission from a 0.5 cm Ag-Na ion-exchanged waveguide formed in the stock glass.

Further, the green-light emission observed in both of these waveguides indicates that the upconversion process and/or ESA occurring at the pump state for Er^{3+} ions (Sec. 2.3.2 and 2.3.3). Figure 5.13 is a photograph showing the green light emission throughout the length of a 0.5 cm waveguide in the stock glass. A study of the intensity of the green emission as a function of pump power could identify the process responsible. In ESA, since only one excited ion is involved, the green emission would increase linearly with the pump power. For upconversion, since two excited ions are involved, the emission would vary quadratically with pump power. An attempt to measure the transmitted green emission was unsuccessful. The intensity was found to be below the noise level (or no peak was found around 520 nm) in the scanned spectrum that was obtained using a monochromator (insertion loss > 10 dB). An available narrow band filter (520 nm, FWHM 92 nm) was used to isolate the green light; however, the pump still wasn't extinguished and dominated the green emission at the detector.

6. Conclusions

The main goal of this thesis was the development of Erbium/Ytterbium co-doped planar waveguide amplifiers for the possible integration with other passive devices in all-optical integrated circuits. High-gain short amplifiers are mostly preferred for applications requiring high-density optical integrated circuits. Thus, the waveguides need to be heavily doped with Erbium ions and more pump power is accordingly required to realize the optimum population inversion.

A numerical model for the waveguide amplifier was developed to predict the amplification characteristics in terms of various parameters such as concentration levels of the active ions, waveguide length, and pump power levels. According to simulation results, the gain performance of purely Erbium-doped amplifiers is severely affected at high concentration levels due to the upconversion effects. When the amplifiers are co-doped with Ytterbium the upconversion effect is noticeably reduced. Ytterbium ions dominantly absorb the pump and populate the metastable state of Er ions through an efficient energy transfer process to the ground state Er ions. Further, the pump power required for maximum gain or the gain saturation is also greatly reduced in Er/Yb co-doped amplifiers compared to that in purely Er-doped amplifiers, where in order to maintain the population inversion (or to compete with the upconversion process) much higher pump powers are needed. Simulation results also suggest that the amplifier gain can be increased by realizing longer waveguides. However, for a given pump power, there exists an optimum length for the maximum gain and the optimum length increases with increasing pump powers.

With a view to developing waveguide amplifiers, commercially available Er/Yb co-doped multi-component phosphate laser glasses were obtained. Phosphate-based glass was chosen among some other oxide glasses since, in the past, it has been shown to offer better material properties such as even distribution of active ions at high doping levels which minimizes the upconversion effect, and longer lifetime for Er ions in the metastable state. Buried channel waveguides were formed on the Er/Yb co-doped bulk glasses by using the field assisted silver-sodium ion-exchange technique. At a signal wavelength of 1533.5 nm, 1.36 dB of internal gain was achieved in a 0.5 cm waveguide

at 60 mW of pump power. The background or the scattering loss in this waveguide was around 0.24 dB/cm.

The result obtained in this work is listed in Table 6.1 along with other published results obtained to date of Er-doped waveguide amplifiers using oxide glasses.

Table 6.1 The results achieved in this work is listed along with some other results reported to date on Er-doped waveguide amplifiers.

Host material	Silicate glass (Er/Yb)	Silicate glass (Er)	Phosphate-glass (Er/Yb)	Phosphate-glass (Er/Yb)	Phosphate-glass (Er)
Fabrication	Ag^+- Na^+ ion exchange	Rf sputtered	Ag^+- Na^+ ion exchange	Ag^+- Na^+ ion exchange	Rf sputtered
Er^{3+} conc. (10^{20} cm^{-3})	0.4	NA*	1.6	1.5	5.3
λ_{pump} (nm)	980	1549	980	980	980
Pump power (mW)	120 (bi-directional)	~ 150	180	60	66
Internal gain/length (in dB/cm)	3.5 dB/4.2 cm (0.8)	18.3 dB/14 cm (1.3)	16.5 dB/9 cm (~ 1.8)	1.4 dB/0.5 cm (~ 2.8)	4.1 dB/1 cm (4.1)
Reference	[9]	[12]	[8]	This work	[11]

* Not available in the reference.

6.1 Future Work

To continue the work done in this thesis, the next appropriate step would be optimizing the gain in the ion-exchanged waveguides. An optimization study through modeling, however, will require all the relevant amplifier parameters.

Modeling the ion-exchanged waveguide amplifier fabricated and best fitting the calculated gain with the measured data will reveal the unknown material parameters such as upconversion and cross-relaxation coefficients. The major obstacle to this step will be finding the index profiles in these electric field assisted ion-exchanged channel waveguides. The index profile in the vertical direction can be easily estimated from a

similar ion-exchanged slab waveguide by using the prism coupling technique [9]. To determine the index-profile in the direction of side diffusion, a quantitative chemical analysis can be done to obtain the silver concentration profile across the waveguide. This data can then be converted to index-profile with the known relationship between concentration and index profile in the vertical direction.

The knowledge of the material parameters and the waveguide structure can then be used to optimize the gain in the waveguides in terms of adjustable parameters such as the waveguide length and the pump power. Also, the upconversion coefficients, estimated in waveguides formed in both glasses (two different concentration levels), will lead to find out the suitability of this commercially available glass in realizing efficient amplifiers.

References

[1] P. Camy, J. E. Roman, F.W. Willems, M. Hempstead, J. C. van der Plaats, C. Preal, A. Beguin, A. M. J. Koonen, J. S. Wilkinson, and C. Lerminiaux, " Ion-exchanged planar lossless splitter at 1.5 μm," Electron. Lett. , Vol. 32, No. 4, 1996, pp. 321-323.

[2] D. Barbier, M. Ratty, F. S. Andre, G. Clauss, M. Trouillon, A. Kevorkian, J- M. P. Delavaux, and E. Murphy, "Amplifying four-Wavelength combiner, based on Erbium-Ytterbium-doped waveguide amplifiers and integrated splitters," IEEE Photon. Technol. Lett. , Vol. 9, No. 3, 1997, pp. 315-317.

[3] A. Polman, "Erbium implanted thin film photonic materials," J. Appl. Phys. Vol. 82, No. 1, 1997, pp. 1-39.

[4] G. N. van den Hoven, E. Snokes, and A. Polman, " Upconversion in Er-implanted Al_2O_3 waveguides," J. Appl. Phys., Vol. 79, No.3, 1996, pp.1258-1266.

[5] R. N.Ghosh, J. Shmulovich, C. F. Kane, M. R. X. Barros, G. Nykolak, A. J. Bruce, and P. C. Becker, " 8-mW Threshold Er^{3+} - Doped Planar Waveguide Amplifier," IEEE Photon. Technol. Lett., Vol. 8, No. 4, 1996, pp. 518-520.

[6] A. Shooshtari, P. Meshkinfam, T. Touam, M. P. Andrews, S. I. Najafi, "Ion-exchanged Er/Yb phosphate glass waveguide amplifiers and lasers," Opt. Eng. Vol. 37, No. 4, 1998, pp. 1188-1192.

[7] D. L. Veasey, D. S. Funk, P. M. Peters, N. A. Sanford, G. E. Obarski, N. Fontaine, M. Young, A. P. Peskin, W. Liu, S. N. Houde-Walter, J. S. Hayden, "Yb/Er-Codoped and Yb-doped waveguide lasers in phosphate glass," J. Non-Crystalline Sol. , Vol. 263&264, 2000, pp. 369-381.

[8] J. M. P. Delavaux, S. Granlund, O. Mizuhara, L. D. Tzeng, D. Barbier, M. Rattay, F. Saint Andre, and A.Kevorkian, "Integrated Optics Erbium-Ytterbium Amplifier System in 10-Gb/s Fiber Transmission Experiment," IEEE Photon. Technol. Lett., Vol. 9, No. 2, 1997, pp. 247-249.

[9] M. Krishnaswamy, "Modeling and fabrication of rare-earth-doped integrated optical waveguide amplifiers," Ph. D. Thesis, University of Alberta, Canada, 1998.

[10] Y. Yan, "Optical Waveguide Amplifiers Based on Er-doped Phosphate Glasses," Ph.D. Thesis, Eindhoven University of Technology, The Netherlands, 1997.

[11] Y. C. Yan, A. J. Faber, and H. de Waal, P. G. Kik, and A. Polman, "Erbium-doped phosphate glass waveguide on silicon with 4.1 dB/cm gain at 1.535 μm," Appl. Phys. Lett., Vol. 20, No. 20, 1997, pp. 2922-2924.

[12] J. Shmulovich, A. J. Bruce, G. Lenz, P. B. Hansen, T. N. Nielsen, D. J. Muehlner, G. A. Bogert, I. Brener, E. J. Laskowski, A. Paunescu, I. Ryazansky, D. C. Jacobson, and A. E. White, "Integrated planar waveguide amplifier with 15 dB net gain at 1550 nm," OFC, San Diego, 1999, PD42-1.

[13] S. Ramachandran and S. G. Bishop, "Excitation of Er^{3+} emission by host glass absorption in sputtered films of Er-doped $Ge_{10}As_{40}Se_{25}S_{25}$ glass," Appl. Phys. Lett., Vol. 73, No. 22, 1998, pp. 3196-3198.

[14] J. Fick, E. J. Knystautas, A. Villeneue, F. Schiettekatte, S. Roorda, and K. A. Richardson, "High photoluminescence in erbium-doped chalcogenide thin films," J. Non-Crystalline Sol., Vol. 272, 2000, pp. 200-208.

[15] L. H. Sloof, A. Polman, M. P. Oude Wolbers, F. C. J. M. van Veggel, D. N. Reinhoudt, and J. W. Hofstraat, "Optical properties of erbium-doped organic polydentate cage complexes," J. Appl. Phys., Vol. 83, No. 1, 1998, pp. 497-503.

[16] G. Nykolak, P. C. Becker, J. Shumulovich, Y. H. Wong, D. J. DiGiovanni, and A. J. Bruce, "Concentration-Dependent $^4I_{13/2}$ Lifetimes in Er^{3+}-Doped Fibers and Er^{3+}-Doped Planar Waveguides," IEEE Photon. Technol. Lett., Vol. 5, No. 9, 1993, pp. 1014-1016.

[17] J. M. P. Delavaux, S. Granlund, O. Mizuhara, L. D. Tzeng, D. Barbier, M. Rattay, F. Saint Andre, and A.Kevorkian, "Integrated Optics Erbium-Ytterbium Amplifier System in 10-Gb/s Fiber Transmission Experiment," IEEE Photon. Technol. Lett., Vol. 9, No. 2, 1997, pp. 247-249.

[18] E. Snokes, G. N. van den Hoven, A. Polman, B. Hendriksen, M. B. J. Diemeer, and F. Priolo, "Cooperative upconversion in erbium-implanted soda-lime silicate glass optical waveguides" J. Opt. Soc. Am. B12, 1995, pp. 1468-1474.

[19] G. N. van den Hoven, E. Snokes, and A. Polman, " Upconversion in Er-implanted Al_2O_3 waveguides," J. Appl. Phys., Vol. 79, No.3, 1996, pp.1258-1266.

[20] T. Kitagawa, K. Hattori, K. Shuto, M. Yasu, M. Kobayashi, and M.Horiguchi, "Amplification in Erbium-doped Silica-based Planar lightwave circuits," OAA, June 24-26, 1992, Snata Fe, New Mexico.

[21] Y. Hibino, T. Kitagawa, M. Shimizu, F. Hanawa, and A. Sugita, " Neodymium-Doped Silica Optical Waveguide Lasers on Silicon Substrate," IEEE Photon. Technol. Lett., Vol. 1, No. 11, 1989, pp. 349- 350.

[22] M. Benatsou, B. Capoen, M. Bouazaoui, W. Tchana, and J. P. Vilcot, " Preparation and characterization of sol-gel derived Er^{3+}: $Al_2O_3-SiO_2$ planar waveguides," Appl. Phys. Lett., Vol. 71, No. 4, 1997, pp. 428-430.

[23] G. R. J. Robertson and P. E. Jessop, " Optical waveguide laser using an rf sputtered Nd:glass film," Appl. Opt., Vol. 30, No. 3, 1991, pp. 276-278.

[24] P. Fournier, P. Meshkinfam, M. A. Fardad, M. P. Andrews and S. I. Najafi, "Potassium ion-exchanged Er-Yb doped phosphate glass amplifier," Electron. Lett. , Vol. 33, No. 04, 1997, pp. 293-295.

[25] R. G. Hunsperger, Integrated Optics: Theory and Technology, Springer-Verlag 1991.

[26] M. Kawachi, "Silica waveguides on silicon and their application to integrated-optic components," Opt. Quantum Electron., Vol. 22, 1990, pp. 391-416.

[27] W. J. Miniscalco, "Erbium-Doped Glasses for Fiber Amplifiers at 1500 nm," J. Lightwave Technol. , Vol. 9, No. 2, 1991, pp. 234-250.

[28] H. Kogelnik, "Theory of Optical Waveguides", Guided-Wave Optoelectronics, Tamir. T, Editor (second edition), Springer-Verlag, 1990.

[29] G. R. Pollock, Fundamentals of Optoelectronics, Irwin, 1995.

[30] D. Marcuse, Theory of Dielectric Optical waveguides, Academic Press, 1974.

[31] P. Lusse, J. Schule, and H.-G. Unger, "Analysis of Vectorial Mode Fields in Optical Waveguides by a New Finite Difference Method", J. Lightwave Technol., Vol. 12, No. 3, 1994, pp. 487-493.

[32] A. Sv. Sudbo "Film mode matching: a versatile numerical method for vector mode field calculations in dielectric waveguides," Pure Appl. Opt., Vol. 2, 1993, pp.211-233.

[33] BBV Software BV, Hengelosestraat 705, 7521 PA Enschede, The Netherlands.

[34] E. Desurvire, Erbium-Doped Fiber Amplifiers, Wiley-Interscience, 1994.

[35] G. P. Agrawal, Fiber-Optic Communication Systems, Wiley-Interscience, 1997.

[36] M. E. Fermann, D. C. Hanna, D. P. Shepherd, P. J. Suni, and J. E. Townsend, "Efficient operation of an Yb- sensitized Er fiber laser at 1.56 μm," Electron. Lett., Vol. 24, No. 18, 1988, pp. 1135-1136.

[37] Schott Glass Technologies Inc., 400 York Avenue, Duryea, PA 18642.

[38] J. Nilsson, P. Scheer, and B. Jaskorzynska, "Modeling and Optimization of Short Yb^{3+} -Sensitized Er^{3+}-Doped Fiber Amplifiers," IEEE Photon. Technol. Lett., Vol. 6, No. 3, 1994, pp. 383-385.

[39] C. Lester, A. Bjarklve, T. Rasmussen, and P. G. Dinesen, Modeling of Yb^{3+} Sensitized Er^{3+} -Doped Silica Waveguide Amplifiers," J. Lightwave Technol., Vol. 13, No. 5, 1995, pp.740-743.

[40] F. Di Pasquale and M. Zoboli, "Analysis of Erbium-Doped Waveguide Amplifiers by a Full-Vectorial Finite-Element Method, "J. Lightwave Technol., Vol. 11, No. 10, 1993, pp. 1565-1573.

[41] F. Di Pasquale and M. Federighi, " Improved Gain Characteristics in High-Concentration Er^{3+}/ Yb^{3+} Codoped Glass Waveguide Amplifiers," IEEE J. Quantum Electron., Vol. 30, No. 9, 1994, pp. 2127-2131.

[42] D. L. Veasey, J. M. Gray, and J. Amin, "Rigorous scalar modeling of Er and Er/Yb-doped waveguide lasers," SPIE Proc., Vol. 2996, 1997, pp. 109-120.

[43] R. V. Ramaswamy and R. Srivastava," Ion-Exchanged Glass Waveguides: A Review," J. Lightwave Technol., Vol. 6, June 1988, pp. 984- 1002.

[44] T. Izawa and H. Nakagome, "Optical waveguide formed by electrically induced migration of ions in glass plates," Appl. Phys. Lett., Vol. 21, No 12, 1972, pp. 584-588.

[45] G. Chartier, P. Collier, A. Guez, P. Jaussaud, and Y. Won, " Graded-index surface or buried waveguides by ion exchange in glass, " Appl. Opt., Vol. 19, No. 7, 1980, pp. 1092-1095.

[46] A. Tervonen, S. Honkanen, and M. Leppihalme, "Control of ion-exchanged waveguide profiles with Ag thin-film sources," J. Appl. Phys., Vol. 62, No. 3, 1987, pp. 759-763.

[47] S. I. Najafi, P. G. Suchoski, and R. V. Ramaswamy, "Silver Film-Diffused Glass Waveguides: Diffusion Process and Optical Properties," IEEE J. Quantum Electron., Vol. QE-22, No. 12, 1986, pp. 2213-2218.

[48] S. Honkanen, A. Tervonen, H. von Bagh, A. Salin, and M. Leppihalme, "Fabrication of ion-exchanged channel waveguides directly into integrated circuit mask plates," Appl. Phys. Lett. , Vol. 51. No. 5, 1987, pp. 296-298.

[49] S. Honkanen, S. I. Najafi, P. Poyhonen, G. Orcel, W. J. Wang, J. Chrostowski, "Silver-film ion-exchanged singlemode waveguides in Er doped phosphate glass," Electron. Lett. , Vol. 27, No. 23, 1991, pp. 2167-2168.

[50] G. H. Charter, P. Jaussaud, A. D. de Oliveira, O. Parriaux, "Optical waveguides fabricated by electric-field controlled ion exchange in glass," Electron. Lett. , Vol. 14, No. 5, 1978, pp. 132-134.

[51] T. Findakly, "Glass waveguides by ion exchange: a review," Opt. Eng., Vol. 24, No. 2, 1985, pp. 244-250.

Appendix

Photolithography and pattern transfer

It is a multi-step process in which the light-induced changes in the solubility of a photosensitive material, called Photo-Resist (PR) is used to transfer the patterns from a photo-mask to the layer in the sample. First, a thin layer of positive photo-Resist (PR), HPR 504 was spin-coated on top of the chrome layer. A standard recipe for pattering HPR 504, available at Microfab was used for this process. Spread speed of 500 rpm for 10 s followed by spin speed of 4000 rpm for 40 s was used for coating the PR and then the sample was soft baked in a vacuum oven for 60 s at 115 °C. The sample and the photo-mask were placed in a 3-axis mask aligner and brought in contact while the patterned side in the photo-mask facing the PR and then exposed to UV light (Intensity ~170 MW/cm^2) for 4 seconds. A mask is a glass plate with a very thin patterned layer of chrome on one side. The mask used in this process which was patterned by e-beam writing had clear regions in chrome the layer (step 2 in Figure 4.4), corresponding to the openings needed for Ag diffusion in the sample. After the UV exposure, the sample was immersed in a developer (MICROPOSIT 354) for roughly 20 second and was then rinsed and cleaned with water. The regions in PR which were exposed to the UV light became soluble in the developer and as seen in step 3, Figure 4.4, narrow opened strips were formed on the PR.

Next, the sample was dipped into the chrome etchent (HNO$_3$) till the chrome was etched down to the glass surface through the openings in the PR. Then the sample was cleaned with acetone to remove all PR remaining in unexposed regions. As shown in step 4, the chrome layer has been selectively removed to form openings needed for Ag diffusion.

76